NASA/CR—1998-207927

HOTCFGM-1D: A Coupled Higher-Order Theory for Cylindrical Structural Components With Through-Thickness Functionally Graded Microstructures

Marek-Jerzy Pindera
University of Virginia, Charlottesville, Virginia

Jacob Aboudi
Tel-Aviv University, Tel-Aviv, Israel

Prepared under Contract NAS3–96052

National Aeronautics and
Space Administration

Lewis Research Center

June 1998

Acknowledgments

The support for this work was provided by the NASA Lewis Research Center through the contract NAS3–96052. The authors thank Dr. Steven M. Arnold of the NASA Lewis Research Center, the technical monitor of this contract, for his valuable suggestions and comments in the course of this investigation.

Available from

NASA Center for Aerospace Information
7121 Standard Drive
Hanover, MD 21076
Price Code: A04

National Technical Information Service
5287 Port Royal Road
Springfield, VA 22100
Price Code: A04

PREFACE

This report summarizes the work performed under the contract **NAS3-96052** during the FY97 funding period. The objective of this three-year project was to develop and deliver to NASA Lewis one-dimensional and two-dimensional higher-order theories, and related computer codes, for the analysis, optimization and design of cylindrical functionally graded materials/structural components for use in advanced aircraft engines (e.g., combustor linings, rotor disks, heat shields, blisk blades). To satisfy this objective, a quasi one-dimensional version of the higher-order theory, **HOTCFGM-1D**, and four computer codes based on this theory, for the analysis, design and optimization of cylindrical structural components functionally graded in the radial direction were developed. The theory is applicable to thin multi-phased composite shells/cylinders subjected to macroscopically axisymmetric thermomechanical and inertial loading applied uniformly along the axial direction such that the overall deformation is characterized by a constant average axial strain. The reinforcement phases are uniformly distributed in the axial and circumferential directions, and arbitrarily distributed in the radial direction, thereby allowing functional grading of the internal reinforcement in this direction.

The three computer codes *fgmp.tube.f*, *fgmp.homog.tube.f*, and *fgm.gvips.tube.f* are research-oriented codes for investigating the effect of functionally graded architectures, as well as the properties of the multi-phase reinforcement, in thin shells subjected to axisymmetric thermomechanical and inertial loading, on the internal temperature, stress and (inelastic) strain fields. The reinforcement distribution in the radial direction is specified by the user. The thermoelastic and inelastic properties of the individual phases can vary with temperature. The inelastic phases are presently modeled either by the incremental plasticity theory (within *fgmp.tube.f*), or GVIPS unified viscoplasticity theory (within *fgm.gvips.tube.f*). A homogenization capability within *fgmp.homog.tube.f* admits the inclusion of heterogeneous phases. The computer code *fgmp.tube.opt.f* combines the major analysis module resident in *fgmp.tube.f* with a commercially-available optimization algorithm, and enables the user to identify radial distributions of the reinforcement phase that minimize (or maximize) user-defined objective functions such as internal moments, resultants or plastic strains.

Notice: The *fgmp.tube.f*, *fgmp.homog.tube.f*, *fgm.gvips.tube.f*, and *fgmp.tube.opt.f* codes are being delivered to the NASA-Lewis Research Center strictly as research tools. The authors of the codes do not assume liability for application of the codes beyond research needs. Any questions or related items concerning these computer codes can be directed to either Professor Marek-Jerzy Pindera at the Civil Engineering & Applied Mechanics Department, University of Virginia, Charlottesville, VA 22903 (Tel: 804-924-1040, e-mail: marek@virginia.edu), or Professor Jacob Aboudi at the Department of Solid Mechanics, Materials & Structures, Faculty of Engineering, Tel-Aviv University, Ramat Aviv, Tel-Aviv 69978, Israel (Tel: 972-3-640-8131, e-mail: aboudi@eng.tau.ac.il).

TABLE OF CONTENTS

1.0 INTRODUCTION

This final report summarizes the work funded under the contract **NAS3-96052** during the FY97 funding period. The objective of this three-year project was to develop and deliver to NASA Lewis one-dimensional and two-dimensional higher-order theories, and related computer codes, for the analysis, optimization and design of cylindrical functionally graded materials/structural components for use in advanced aircraft engines (e.g., combustor linings, rotor disks, heat shields, blisk blades). These theories will enable the designer to enhance the performance of aircraft engine structural components through the use of functionally graded architectures/microstructures. The analytical approach employed in the theories' construction explicitly couples microstructural and macrostructural effects in cylindrical bodies of revolution wherein the reinforcement phase or phases are spatially varied to improve thermomechanical performance (deformation, thermal fatigue resistance and life). At present, functionally graded structural components cannot be analyzed accurately using the standard micromechanics approach based on the representative volume concept coupled with macrostructural analysis in a noninteractive manner. Such coupling is explicitly taken into account in the present theoretical development, thereby providing the capability and means (through the related computer code(s)) to accurately analyze the response of cylindrical functionally graded structural components.

The work performed during the FY97 funding period resulted in the development of a quasi one-dimensional version of the higher-order theory, **HOTCFGM-1D**, and four computer codes based on this theory, for the analysis, design and optimization of cylindrical structural components functionally graded in the radial direction. The theory is applicable to multi-phased composite thin shells/cylinders subjected to macroscopically axisymmetric thermomechanical and inertial loading applied uniformly along the axial direction such that the overall deformation is characterized by a constant average axial strain and stress, Fig. 1. The reinforcement phases are uniformly distributed in the axial and circumferential directions, and arbitrarily distributed in the radial direction, thereby allowing functional grading of the internal reinforcement in this direction. They can be in the form of continuous fibers, oriented in the axial or circumferential direction, or discontinuous inclusions. The development of the quasi one-dimensional version includes inertial body forces in order to account for the effect of rotation, in addition to externally applied loads, and through-thickness temperature gradients. The applied boundary conditions can be in the form of imposed temperatures on the inner and outer surfaces and/or radial pressure/displacement. Further, the development has been carried out in a manner that facilitates incorporation of nonisothermal inelastic constitutive and damage theories within any individual constituent. At present, classical incremental plasticity theory and GVIPS unified viscoplasticity theory are available within the developed computer codes.

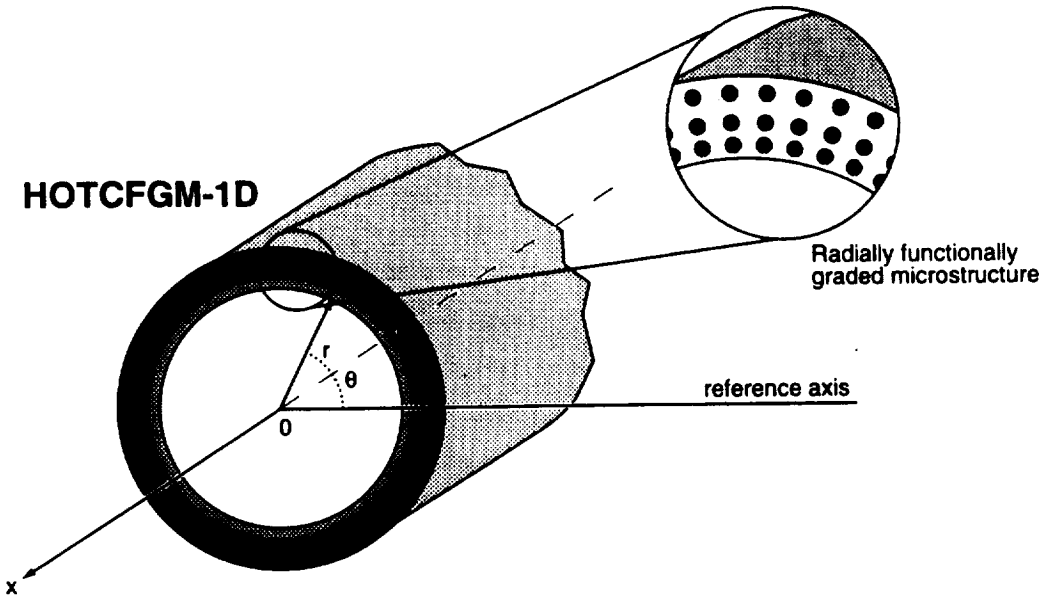

Figure 1. A geometric model for the cylindrical higher-order theory HOTCFGM-1D.

The three computer codes *fgmp.tube.f*, *fgmp.homog.tube.f*, and *fgm.gvips.tube.f* are research-oriented codes for investigating the effect of functionally graded architectures, as well as the properties of the multi-phase reinforcement, in thin shells subjected to axisymmetric thermomechanical and inertial loading, on the internal temperature, stress and (inelastic) strain fields. The reinforcement distribution in the radial direction is specified by the user. The thermoelastic and inelastic properties of the individual phases can vary with temperature and the elastic phases can be either isotropic or transversely isotropic. In the latter case, the axis of symmetry can be in the radial, circumferential or axial direction. The inelastic phases can be modeled either by the classical plasticity (within *fgmp.tube.f*) [1], or GVIPS unified viscoplasticity theory (within *fgm.gvips.tube.f*) [2]. A homogenization capability within *fgmp.homog.tube.f* admits the inclusion of heterogeneous phases.

The computer code *fgmp.tube.opt.f* combines the major analysis module in *fgmp.tube.f* with the commercially-available optimization code *DOT*[1] [3]. The total optimization package enables the user to identify radial distributions of the reinforcement phase that minimize (or maximize) user-defined objective functions such as internal moments, resultants or plastic strains.

[1]License for the *DOT* source code must be purchased separately from VMA Engineering (Vanderplaats, Miura & Associates, Inc.), 5960 Mandarin Ave., Suite F, Goleta, CA 93117. Phone: (805) 967-0058.

2.0 ANALYTICAL FOUNDATIONS OF HOTCFGM-1D

The developed theory is a significant extension of the theories previously constructed by the authors for the analysis and design of functionally graded plates under NASA-Lewis funding (see Ref. [4] for appropriate references and summary of accomplishments). The analytical framework of the quasi one-dimensional version of the higher-order theory for cylindrical shells under axisymmetric loading is based on a second order representation of temperature and displacement fields within the subvolumes used to characterize the material's functionally graded microstructure, volumetric averaging of the various field quantitites within these subvolumes, and subsequent satisfaction of the field equations within each subvolume in a volumetric sense, together with the imposition of boundary and continuity conditions in an average sense between adjacent subvolumes. This results in a system of algebraic equations for the unknown coefficients that govern the temperature and displacement field in the individual subvolumes of a functionally graded cylinder under axisymmetric loading due to through-thickness temperature gradient, internal/external pressure and inertial body forces caused by steady rotation. The algebraic system of equations is implicitly nonlinear due to the use of nonisothermal inelastic constitutive theories (incremental plasticity and GVIPS unified viscoplasticity) for the materials occupying various subvolumes of the functionally graded microstructure. When the classical plasticity equations are used to describe the inelastic material behavior, an interative scheme is employed to solve the nonlinear system of equations [1]. A brief outline of the construction of the one-dimensional higher-order theory for cylindrical functionally graded structural components under steady-state thermomechanical and inertial loading is provided below.

2.1 Analytical Model

The microstructure of the heterogeneous cylindrical structural element shown in Fig. 1 is discretized into M cells spanning the r-direction. The generic cell (p) used to construct the composite consists of eight subcells designated by the triplet ($\alpha\beta\gamma$), where each index α, β, γ takes on the values 1 or 2 which indicate the relative position of the given subcell along the r, θ and z axis, respectively. The index p, whose range is p = 1, 2,...,M, identifies the generic cell in the r-direction. The dimensions of the generic cell along the periodic θ and z directions, h_1, h_2, and l_1, l_2, are fixed for the given configuration, whereas the dimensions along the r axis or the functionally graded direction, $d_1^{(p)}$, $d_2^{(p)}$, can vary in an arbitrary fashion.

For the specified axisymmetric thermomechanical loading applied in the $r-\theta$ plane, an approximate solution for the temperature and displacement fields has been constructed by first approximating the temperature distribution in each subcell of a generic cell using a quadratic expansion in the local coordinates $\bar{r}^{(\alpha)}$, $\bar{\theta}^{(\beta)}$, $\bar{z}^{(\gamma)}$,

$$T^{(\alpha\beta\gamma)} = T^{(\alpha\beta\gamma)}_{(000)} + \bar{r}^{(\alpha)} T^{(\alpha\beta\gamma)}_{(100)} + \frac{1}{2}(3\bar{r}^{(\alpha)2} - \frac{d_\alpha^{(p)2}}{4}) T^{(\alpha\beta\gamma)}_{(200)} + \frac{1}{2}(3\bar{y}^{(\beta)2} - \frac{h_\beta^{(q)2}}{4}) T^{(\alpha\beta\gamma)}_{(020)}$$

$$+ \frac{1}{2}(3\bar{z}^{(\gamma)2} - \frac{l_\gamma^2}{4}) T^{(\alpha\beta\gamma)}_{(002)} \qquad (1)$$

where $\bar{y}^{(\beta)} = R^{(\alpha\beta\gamma)}\bar{\theta}^{(\beta)}$ and $R^{(\alpha\beta\gamma)}$ is the distance from the origin of the r – θ – z coordinate system to the center of the (αβγ) subcell. Given the five unknown coefficients associated with each subcell (i.e., $T^{(\alpha\beta\gamma)}_{(000)}$, ... , $T^{(\alpha\beta\gamma)}_{(002)}$) and eight subcells within each generic cell, 40M unknown quantities must be determined for a composite with M rows of cells in the r-direction containing arbitrarily specified materials. These quantities are determined by first satisfying the heat conduction equation,

$$\frac{\partial q_r^{(\alpha\beta\gamma)}}{\partial \bar{r}^{(\alpha)}} + \frac{q_r^{(\alpha\beta\gamma)}}{R^{(\alpha\beta\gamma)} + \bar{r}^{(\alpha)}} + \frac{\partial q_\theta^{(\alpha\beta\gamma)}}{\partial \bar{y}^{(\beta)}} + \frac{\partial q_z^{(\alpha\beta\gamma)}}{\partial \bar{z}^{(\gamma)}} = 0 \qquad (2)$$

as well as the first and second moment of this equation in each subcell in a volumetric sense in view of the employed temperature field approximation. The components $q_i^{(\alpha\beta\gamma)}$ (i = r, θ, z) of the heat flux vector in the the subcell (αβγ) of the (p)th cell in eqn (2) are derived from the temperature field according to

$$q_r^{(\alpha\beta\gamma)} = -k_r^{(\alpha\beta\gamma)} \frac{\partial T^{(\alpha\beta\gamma)}}{\partial \bar{r}^{(\alpha)}}, \quad q_\theta^{(\alpha\beta\gamma)} = -k_\theta^{(\alpha\beta\gamma)} \frac{\partial T^{(\alpha\beta\gamma)}}{\partial \bar{y}^{(\beta)}}, \quad q_z^{(\alpha\beta\gamma)} = -k_z^{(\alpha\beta\gamma)} \frac{\partial T^{(\alpha\beta\gamma)}}{\partial \bar{z}^{(\gamma)}} \qquad (3)$$

where $k_i^{(\alpha\beta\gamma)}$ are the coefficients of heat conductivity of the material in the subcell (αβγ).

Subsequently, continuity of heat flux and temperature has been imposed in an average sense at the interfaces separating adjacent subcells, as well as neighboring cells. Fulfillment of these field equations and continuity conditions, together with the imposed thermal boundary conditions at the top and bottom, and left and right surfaces of the composite, has provided the necessary 40M equations for the 40 unknown coefficients in the temperature field expansion of the form:

$$\boldsymbol{\kappa}\, \mathbf{T} = \mathbf{t} \qquad (4)$$

where the structural thermal conductivity matrix $\boldsymbol{\kappa}$ contains information on the geometry and thermal conductivities of the subcells (αβγ) in the M cells spanning the functionally graded r-direction, the thermal coefficient vector T contains the unknown coefficients that describe the

thermal field in each subcell, i.e., $\mathbf{T} = [\, \mathbf{T}_1^{(111)}, \ldots, \mathbf{T}_M^{(222)} \,]$ where $\mathbf{T}_p^{(\alpha\beta\gamma)} = [\, T_{(000)}, T_{(100)}, T_{(200)}, T_{(020)}, T_{(002)} \,]_p^{(\alpha\beta\gamma)}$, and the thermal force vector $\mathbf{t}$ contains information on the thermal boundary conditions.

Once the temperature field is known, the resulting displacement and stress fields are determined by approximating the displacement field in each subcell of a generic cell by a quadratic expansion in the local coordinates $\bar{r}^{(\alpha)}$, $\bar{y}^{(\beta)}$, and $\bar{z}^{(\gamma)}$ as follows:

$$u_r^{(\alpha\beta\gamma)} = W_{1(000)}^{(\alpha\beta\gamma)} + \bar{r}^{(\alpha)} W_{1(100)}^{(\alpha\beta\gamma)} + \frac{1}{2}(3\bar{r}^{(\alpha)2} - \frac{1}{4} d_\alpha^{(p)2}) W_{1(200)}^{(\alpha\beta\gamma)} + \frac{1}{2}(3\bar{y}^{(\beta)2} - \frac{1}{4} h_\beta^{(q)2}) W_{1(020)}^{(\alpha\beta\gamma)}$$

$$+ \frac{1}{2}(3\bar{z}^{(\gamma)2} - \frac{1}{4} l_\gamma^2) W_{1(002)}^{(\alpha\beta\gamma)} \tag{5}$$

$$u_\theta^{(\alpha\beta\gamma)} = \bar{y}^{(\beta)} W_{2(010)}^{(\alpha\beta\gamma)} \tag{6}$$

$$u_z^{(\alpha\beta\gamma)} = \bar{z}^{(\gamma)} W_{3(001)}^{(\alpha\beta\gamma)} \tag{7}$$

where the unknown coefficients $W_{i(lmn)}^{(\alpha\beta\gamma)}$ (i = 1, 2, 3) are determined from conditions similar to those employed in the thermal problem. In this case, there are 56 unknown quantities in a generic cell (p). The determination of these quantities parallels that of the thermal problem with the thermal equations and quantities replaced by their mechanical analogues as briefly described below.

First, the heat conduction equation is replaced by the three equilibrium equations,

$$\frac{\partial \sigma_{rr}^{(\alpha\beta\gamma)}}{\partial \bar{r}^{(\alpha)}} + \frac{\partial \sigma_{r\theta}^{(\alpha\beta\gamma)}}{\partial \bar{y}^{(\beta)}} + \frac{\partial \sigma_{rz}^{(\alpha\beta\gamma)}}{\partial \bar{z}^{(\gamma)}} + \frac{\sigma_{rr}^{(\alpha\beta\gamma)} - \sigma_{\theta\theta}^{(\alpha\beta\gamma)}}{R^{(\alpha\beta\gamma)} + \bar{r}^{(\alpha)}} + F_r^{(\alpha\beta\gamma)} = 0 \tag{8}$$

$$\frac{\partial \sigma_{rz}^{(\alpha\beta\gamma)}}{\partial \bar{r}^{(\alpha)}} + \frac{\partial \sigma_{rz}^{(\alpha\beta\gamma)}}{\partial \bar{y}^{(\beta)}} + \frac{\partial \sigma_{zz}^{(\alpha\beta\gamma)}}{\partial \bar{z}^{(\gamma)}} + \frac{\sigma_{rz}^{(\alpha\beta\gamma)}}{R^{(\alpha\beta\gamma)} + \bar{r}^{(\alpha)}} = 0 \tag{9}$$

$$\frac{\partial \sigma_{r\theta}^{(\alpha\beta\gamma)}}{\partial \bar{r}^{(\alpha)}} + \frac{\partial \sigma_{\theta\theta}^{(\alpha\beta\gamma)}}{\partial \bar{y}^{(\beta)}} + \frac{\partial \sigma_{\theta z}^{(\alpha\beta\gamma)}}{\partial \bar{z}^{(\gamma)}} + \frac{2}{R^{(\alpha\beta\gamma)} + \bar{r}^{(\alpha)}} \sigma_{r\theta}^{(\alpha\beta\gamma)} = 0 \tag{10}$$

where $F_r^{(\alpha\beta\gamma)}$ is the component of the body force due to the radial acceleration. The components of the stress tensor, assuming that the material occupying the subcell $(\alpha\beta\gamma)$ of the (p)th cell is orthotropic, are related to the strain components through the generalized Hooke's law:

$$\sigma_{ij}^{(\alpha\beta\gamma)} = c_{ijkl}^{(\alpha\beta\gamma)} \left(\varepsilon_{kl}^{(\alpha\beta\gamma)} - \varepsilon_{kl}^{in(\alpha\beta\gamma)} \right) - \Gamma_{ij}^{(\alpha\beta\gamma)} T^{(\alpha\beta\gamma)} \tag{11}$$

where $c_{ijkl}^{(\alpha\beta\gamma)}$ are the elements of the stiffness tensor, $\varepsilon_{ij}^{in(\alpha\beta\gamma)}$ are the inelastic strain components, and the elements $\Gamma_{ij}^{(\alpha\beta\gamma)}$ of the so-called thermal tensor are the products of the stiffness tensor and the thermal expansion coefficients. For isotropic elastic or inelastic materials eqn (11) reduces to:

$$\sigma_{ij}^{(\alpha\beta\gamma)} = \lambda_{(\alpha\beta\gamma)} \varepsilon_{kk}^{(\alpha\beta\gamma)} \delta_{ij} + 2\mu_{(\alpha\beta\gamma)} \varepsilon_{ij}^{(\alpha\beta\gamma)} \delta_{ij} - 2\mu_{(\alpha\beta\gamma)} \varepsilon_{ij}^{in(\alpha\beta\gamma)} - \Gamma_{ij}^{(\alpha\beta\gamma)} T^{(\alpha\beta\gamma)} \tag{12}$$

where $\lambda_{(\alpha\beta\gamma)}$ and $\mu_{(\alpha\beta\gamma)}$ are the Lame's constants of the material filling the given subcell $(\alpha\beta\gamma)$. The components of the strain tensor in the individual subcells are, in turn, obtained from the strain-displacement relations.

Second, the continuity of tractions and displacements at the various interfaces replaces the continuity of heat fluxes and temperature. Finally, the boundary conditions involve the appropriate mechanical quantities.

Application of the above equations and conditions in a volumetric and average sense, respectively, has produced a system of 56M algebraic equations in the field variables within the cells of the functionally graded composite of the form:

$$\mathbf{K\,U = f + g} \tag{13}$$

where the structural stiffness matrix **K** contains information on the geometry and thermomechanical properties of the individual subcells $(\alpha\beta\gamma)$ within the cells comprising the functionally graded composite, the displacement coefficient vector **U** contains the unknown coefficients that describe the displacement field in each subcell, i.e., $\mathbf{U} = [\, \mathbf{U}_1^{(111)}, \ldots, \mathbf{U}_M^{(222)} \,]$ where $\mathbf{U}_p^{(\alpha\beta\gamma)} = [\, W_{1(000)}, \ldots, W_{3(001)} \,]_p^{(\alpha\beta\gamma)}$, and the mechanical force vector **f** contains information on the boundary conditions, body forces and the thermal loading effects generated by the applied temperature or heat flux. In addition, the inelastic force vector **g** appearing on the right hand side of eqn (13) contains inelastic effects given in terms of the integrals of the inelastic strain distributions $\varepsilon_{ij}^{in(\alpha\beta\gamma)}(\bar{r}^{(\alpha)}, \bar{y}^{(\beta)}, \bar{z}^{(\gamma)})$ that are represented by the coefficients $R_{ij(l,m,n)}^{(\alpha\beta\gamma)}$,

$$\frac{R_{ij(l,m,n)}^{(\alpha\beta\gamma)}}{\mu_{(\alpha\beta\gamma)}} = \frac{\sqrt{(1+2l)(1+2m)(1+2n)}}{4} \int_{-1}^{1}\int_{-1}^{1}\int_{-1}^{1} \varepsilon_{ij}^{in(\alpha\beta\gamma)} P_l(\zeta_1^{(\alpha)}) P_m(\zeta_2^{(\beta)}) P_n(\zeta_3^{(\gamma)}) d\zeta_1^{(\alpha)} d\zeta_2^{(\beta)} d\zeta_3^{(\gamma)} \tag{14}$$

where the non-dimensionalized variables $\zeta_i^{(\cdot)}$'s, defined in the interval $-1 \le \zeta_i^{(\cdot)} \le 1$, are given in terms of the local subcell coordinates as follows: $\zeta_1^{(\alpha)} = \bar{r}^{(\alpha)} / (d_\alpha^{(p)}/2)$, $\zeta_2^{(\beta)} = \bar{y}^{(\beta)} / (h_\beta^{(q)}/2)$, and $\zeta_3^{(\gamma)} = \bar{z}^{(\gamma)} / (l_\gamma/2)$, and where $P_l(\cdot)$, $P_m(\cdot)$, and $P_n(\cdot)$ are Legendre polynomials of orders l, m and n. These integrals depend implicitly on the elements of the displacement coefficient vector **U**, requiring an incremental solution of eqn (13) at each point along the loading path. The formulation is sufficiently general to admit either rate-independent incremental plasticity or rate-dependent unified viscoplasticity constitutive theories.

2.2 Optimization Scheme

The solution procedure for the inelastic response of a functionally graded cylinder described in the preceding section provides a mechanism for extracting the magnitudes of temperature, stress and (plastic) strain fields in the individual phases for the prescribed values of the reinforcement's dimensions, radial distributions and material parameters. In order to efficiently select those geometric arrangements that yield a desirable or optimal temperature, stress or (plastic) strain patterns, it is necessary to incorporate the outlined solution procedure into an optimization algorithm. This is readily accomplished since closed-form expressions, eqns (4) and (13), are available that describe the response of the functionally graded cylinder cylinder to the specified loading in terms of the cylinder's geometric parameters and the constituent materials' properties. By varying the geometric parameters or *design variables* in an optimization scheme, optimal radial distributions of the reinforcement phases can be determined that minimize or maximize the specified objective function. The optimization algorithm to be described in this section, together with the analysis algorithm described earlier, constitute the two major modules in the optimization code *fgmp.tube.opt.f* developed under the terms of the contract.

The optimization problem is, in general, formulated as follows,

Minimize or maximize the user-defined objective function $F(\mathbf{X})$, *where* $\mathbf{X}$ *is a set of design variables, subject to the constraints* $g_j(\mathbf{X}) \le 0$ *where* $j = 1, \ldots, M$, *with the following side constraints,* $X_i^l \le X_i \le X_i^u$ *where* $i = 1, \ldots, N$, *with u and l denoting upper and lower limits for each design variable* X_i.

In order to allow the user sufficient flexibility to define a wide range of optimization problems, the objective function $F(\mathbf{X})$ and the constraint functions $g_j(\mathbf{X})$ within *fgmp.tube.opt.f* are user-constructed functions that have to be coded into the computer program. The design variables employed in *fgmp.tube.opt.f* are those parameters that describe the reinforcement phases' radial distributions, namely the radial spacings between individual fibers/inclusions. Finally, the

side constraints (i.e., lower and upper bounds) that can be imposed on the design variables should be commensurate with the physical problem at hand, such as minimum radial distances between the reinforcement phases.

The optimization algorithm incorporated in the software package *DOT* is based on the method of feasible directions, Vanderplaats [5]. This method, briefly outlined here, essentially searches the n-dimensional design variable space in an iterative manner along the constraint boundaries for the "global optimum". Once an initial set of design variables, $\mathbf{X}_0$ is specified by the user, the search procedure is carried out according to the following algorthim,

$$\mathbf{X}^q = \mathbf{X}^{q-1} + \alpha^* \mathbf{S}^q \tag{15}$$

where q is the iteration number, $\mathbf{X}^q$ is the vector of design variables at the q–th iteration, $\mathbf{S}^q$ is the current direction in the n-dimensional design variable space, and α^* is the distance travelled along the search direction specified by **S**. In this method, the **usable sector** is defined as any direction **S** in the design space that improves the objective function. This is defined mathematically in terms of the inequality,

$$\nabla \mathbf{F}(\mathbf{X}_0) \cdot \mathbf{S} \leq 0 \tag{16}$$

where $\nabla \mathbf{F}(\mathbf{X}_0)$ is the gradient of the objective function at the given design point. The **feasible sector** is defined in any direction **S** in the design space which does not violate the design constraints. This is defined mathematically by the following inequality,

$$\nabla \mathbf{g}_1(\mathbf{X}_0) \cdot \mathbf{S} < 0 \tag{17}$$

where $\nabla \mathbf{g}_1(\mathbf{X}_0)$ is the gradient of the constraint function at the present design point. The intersection of the two sectors is called **usable-feasible** sector. These sectors are indicated in Fig. 2. Any search direction **S** in this sector will improve the design, and at the same time, will not violate any of the design constraints. Once a suitable search direction is found, a one-dimensional search is performed to locate the distance α^* to the minimum (or maximum) in that direction. The newly located design is then defined as the next design point. This process is repeated at each design point until the convergence criteria is reached (in this case the Kuhn-Tucker conditions).

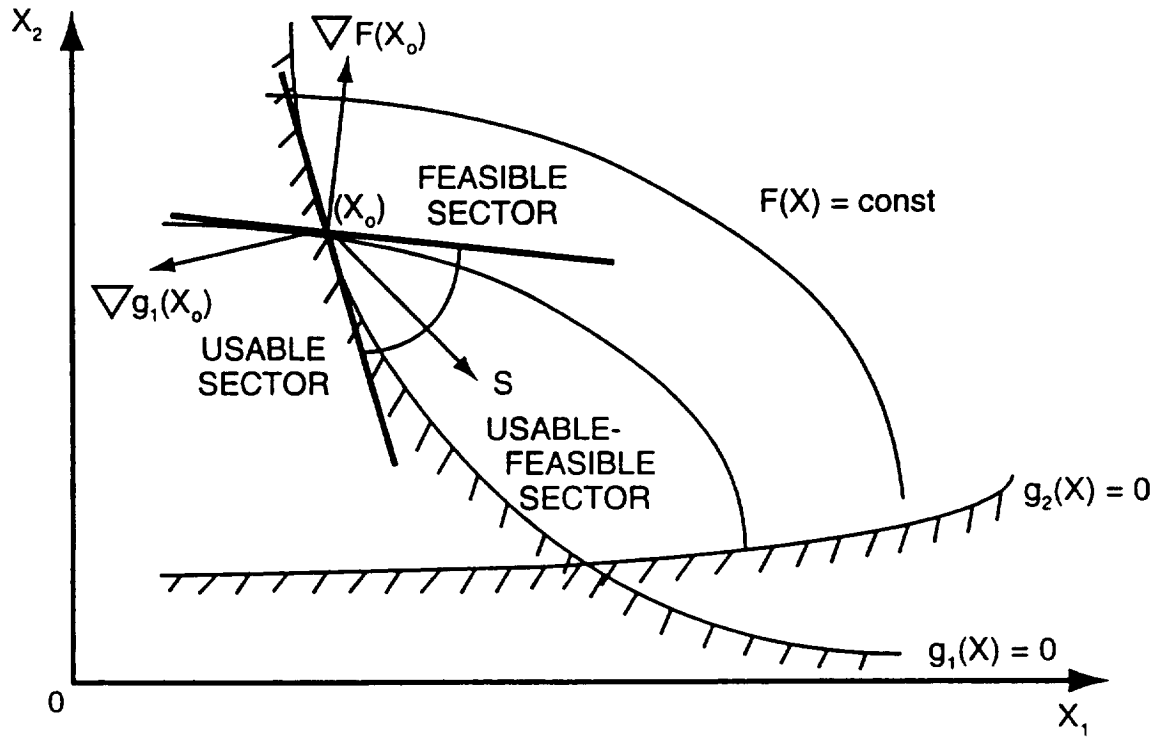

Figure 2. Schematic illustrating the method of feasible directions for two design variables (after Vanderplaats [5]).

3.0 DELIVERABLES

Brief descriptions of the features and capabilities of the computer codes *fgmp.tube.f*, *fgmp.homog.tube.f*, *fgm.gvips.tube.f*, and *fgmp.tube.opt.f* for the analysis and design of radially functionally graded cylinders, delivered to the NASA-Lewis Research Center in fulfillment of the terms of the contract **NAS3-96052** are provided in the following sections.

3.1 Analysis Codes

The computer codes *fgmp.tube.f*, *fgmp.homog.tube.f*, and *fgm.gvips.tube.f* enable the user to investigate the internal temperature, stress and (inelastic) strain fields in cylindrical structural components with radial functionally graded reinforcement in the form of continuous fibers or discontinuous inclusions subjected to axisymmetric thermomechanical and inertial loading. Each of these Fortran codes is first compiled in order to generate an executable file called *a.out* which, in turn, is executed by typing the command of the same name at the unix prompt. The code *fgmp.tube.f* is employed when the inelastic material response of the individual homogeneous phases is modeled using the classical incremental plasticity theory, whereas *fgm.gvips.tube.f* is employed for homogeneous phases modeled with the GVIPS unified viscoplasticity theory. The code *fgmp.homog.tube.f* has been developed for modeling functionally graded cylinders containing heterogeneous phases wherein the response of the individual constituents is described by the classical incremental plasticity theory. In this case, the macroscopic response of the heterogeneous phases is calculated using the *generalized method of cells* micromechanics model [6].

The structure of the input data files is similar for these three codes and the definitions of the input variables associated with each READ statement are well-documented directly within the codes. A brief overview of the structure of the input data file is provided below for *fgmp.tube.f* and further elaborated upon in Appendix 1. An example of this input file is given in Appendix 2 for the problem of a rotating SiC/Ti tube investigated in the following section. The structure of the input data files for *fgm.gvips.tube.f* and *fgmp.homog.tube.f* is similar, with appropriate modifications for the slightly different capabilities of these two codes, i.e., use of GVIPS viscoplasticity in place of classical incremental plasticity in the case of *fgm.gvips.tube.f*, and use of heterogeneous phases in place of homogeneous phases in the case of *fgmp.homog.tube.f*.

The data is read from the input file *fgmp.tube.data* and the results are written to the three output files *fgmp.tube.out*, *fgmp.tube.plot*, and *fgmp.tube.plot.anal*. The input data consists of several blocks. Block 1 is designated for the specification of the number of the individual phases, and their temperature-dependent material parameters, that make up the cylinder's functionally graded microstructure. Each phase is homogeneous and can be either elastic or inelastic.

Elastic phases can be either isotropic or transversely isotropic. In the latter case, the axis of symmetry can be in the radial, circumferential or axial direction. Inelastic phases must be isotropic and are modeled by the classical plasticity with isotropic hardening in conjunction with a bilinear representation of the elastoplastic stress-strain curve. Block 2 is designated for the specification of the loading history, which can involve the simultaneous application of temperature, internal and external pressure, average axial stress or uniform axial strain, and steady-state angular velocity in a monotonic manner. As the loading is applied incrementally, information required for the solution of eqns (4) and (13) is also provided in this block (number of load increments and number of iterations at each load increment used in Mendelson's iterative solution of these equations), together with the manner in which the results generated by the program are written to the output files *fgmp.tube.out* and *fgmp.tube.plot* (loading path and geometric locations). Block 3 is designated for the specification of the cylinder architecture and geometry involving the number of cells in the radial and circumferential directions, subcell dimensions within each cell, and the inner radius of the cylinder. The assignment of different phases to the individual subcells is also specified in Block 3. The last block, Block 4, is designated for the specification of the order of Legendre polynomials employed in approximating the plastic strain field in the individual subcells, eqn (13), and the number of collocation points employed to integrate the plastic strains.

The input data is echoed to the output file *fgmp.tube.out*. In addition, this file contains temperature, stress and (plastic) strain fields in the individual subcells at the specified points of the loading history. An example of this output file is given in Appendix 3 for the problem of the previously mentioned rotating SiC/Ti tube. The output file *fgmp.tube.plot* contains temperature, stress and (plastic) strain distributions along the radial direction of the functionally graded cylinder that can be used directly for plotting purposes. The output file *fgmp.tube.plot.anal* contains exact analytical solutions to four elasticity problems of a homogeneous hollow cylinder subjected to thermal and mechanical loading that can be used to verify the accuracy of the higher-order theory. The four solutions involve the following boundary conditions:

- Radial displacement specified on inner surface and radial traction on outer surface
- Radial traction specified on inner and outer surface
- Steady-state angular velocity specified; no applied mechanical loading
- Temperature specified on inner and outer surface; no applied mechanical loading

In all these cases both plane strain and generalized plane strain solution are provided.

The capabilities and options available within the three analysis codes are summarized in Table 1.

Table 1. Capabilities available within the analysis codes.

Type	Description
Functionally graded cylinder geometry	**Reinforcement**: continuous or discontinuous **Spacing**: arbitrarily nonuniform (user-specified) in the radial direction; axially & circumferentially periodic
Constitutive models	**Elastic**: isotropic, transversely isotropic, orthotropic materials **Plastic**: incremental plasticity (Prandtl-Reuss relations) with isotropic hardening and bilinear representation of the elastoplastic stress-strain response (*fgmp.tube.f*) **Viscoplastic**: GVIPS unified viscoplasticity theory for isotropic materials (*fgm.gvips.tube.f*)
Phases	**Homogeneous**: *fgmp.tube.f* and *fgm.gvips.tube.f* codes **Heterogeneous**: *fgmp.homog.tube.f* code
Integration schemes	**Spatial**: successive elastic solutions (incremental plasticity) **Time**: forward Euler integration technique (GVIPS viscoplasticity)
Loading capabilities	**Thermal**: steady-state, through-thickness temperature gradient **Mechanical**: steady-state internal and external pressure, radial displacement, or mixed **Inertial**: steady-state rotation
Predictive capabilities	Through-thickness temperature distributions Through-thickness stress and (plastic) strain distributions

3.2 Optimization Code

The optimization code *fgmp.tube.opt.f* enables the user to identify those optimum functionally graded architectures in cylindrical structural components that minimize (or maximize) user-constructed functions involving temperature, stress and (plastic) strain fields induced by axisymmetric thermomechanical and inertial loading. As indicated in Section 2.2, this is accomplished through variation of the reinforcement's radial spacing. The information generated by the optimization code can, in turn, be employed for design purposes.

In essence, *fgmp.tube.opt.f* is based on two modules, namely: the analysis code based on the developed theory which, in addition to generating the elastoplastic solution to the functionally graded cylinder subjected to specified loading, also controls the execution of the optimization procedure; and the optimization package *DOT*. The data provided during the problem definition stage through the user-supplied input files is subsequently used to generate a solution to the defined elastoplastic boundary-value problem which, in turn, is used as input to the optimization algorithm. The code is first compiled in order to generate an executable file called *a.out* which, in turn, is executed by typing the command of the same name at the unix prompt.

There are two input data files required to run the executable file, namely *fgmp.tube.opt.data.initial* and *fgmp.tube.opt.data*. The input file *fgmp.tube.opt.data.initial* defines the type of optimization problem (minimization or maximization of objective function), method of optimization available within *DOT*, and contains information on the initial values of the design variables (radial spacings between individual reinforcement). The input file *fgmp.tube.opt.data* contains information of the material properties of the individual phases, loading and write options, architecture and dimensions of the cylinder, and how the plastic strain field in eqn (13) is approximated and integrated. The structure of this file is the same as that of *fgmp.tube.data* employed in the code *fgmp.tube.f* and, with the exception of few lines directly relevant to the optimization problem, contains the same information. The structure of these two input files is described in detail in Appendix 4, and examples are given in Appendix 5 for the optimization problem of a rotating SiC/Ti tube investigated in the following section.

The results from the optimization code *fgmp.tube.opt.f* are written to the following three output files: *fgmp.tube.opt.out*, *fgmp.tube.pre.opt.plot*, and *fgmp.tube.opt.plot*. The output file *fgmp.tube.opt.out* contains the echo of the input data, information on the optimization process generated by *DOT*, and initial and final values of the objective function and design variables, as well as temperature, stress and (plastic) strains in the individual subcells at the specified points of the loading history for the initial and optimum design variables. The output file *fgmp.tube.pre.opt.plot* and *fgmp.tube.opt.plot* contain initial and optimum temperature, stress

and (plastic) strain distributions along the radial direction of the functionally graded cylinder, respectively, that can be used directly for plotting purposes.

The capabilities of the analysis module employed in *fgmp.tube.opt.f* are the same as those of *fgmp.tube.f*. Table 2 summarizes the features and capabilities of *fgmp.tube.opt.f*.

Table 2. Capabilities available within the optimization code.

Type	Description
Functionally graded cylinder geometry	**Reinforcement**: continuous or discontinuous **Spacing**: radially nonuniform, axially & circumferentially periodic
Constitutive models	**Elastic**: isotropic, transversely isotropic, orthotropic materials **Plastic**: incremental plasticity (Prandtl-Reuss relations) with isotropic hardening and bilinear representation of the elastoplastic stress-strain response
Phases	**Homogeneous**
Integration schemes	**Spatial**: successive elastic solutions (incremental plasticity)
Loading capabilities	**Thermal**: steady-state, through-thickness temperature gradient **Mechanical**: steady-state internal and external pressure, radial displacement, or mixed **Inertial**: steady-state rotation
Optimization features	**Design variables**: radial spacing between individual continuous or discontinuous inclusions **Objective functions**: circumferential moment, plastic strain, user-defined function **Constraints**: radial spacing, user-defined function

4.0 SUMMARY OF RESEARCH ACTIVITIES AND RESULTS

The development of the aforementioned computer codes was accompanied by the following investigations:

- Code validation
- Investigation of microstructural effects in SiC/Ti tubes subjected to internal pressure and steady-state rotation (coupled versus homogenized approach)
- Optimization of SiC/Ti tubes subjected to internal pressue
- Optimization of rotating SiC/Ti tubes

These investigations demonstrate the superiority of the coupled approach in the analysis of MMC cylindrical components as well as the developed codes' capability as analysis and design tools. The results of these investigations are currently being summarized in a number of conference and refereed journal papers [7,8,9].

The results presented in this section have been generated using the material properties given in Table 3. The inelastic response of the individual phases is modeled using the incremental plasticity theory with isotropic hardening in conjunction with a bilinear representation of the elastoplastic stress-strain response.

Table 3. Thermoelastic and plastic parameters of titanium and nickel alloys, and SiC fiber.

Material	Youngs' Modulus (GPa)	Poisson's ratio	Yield stress	Hardening slope (MPa)
Ti-24Al-11Nb	110.3	0.26	371.6	23.0
NiAl	193.0	0.32	315.1	3.4
SiC	399.9	0.25	-	-

4.1 Validation Studies

Figure 3 illustrates the comparison between the predictions of **HOTCFGM-1D** and an exact analytical solution for a homogeneous Ti-24Al-11Nb tube with an inner radius of 0.02 m and an outer radius of 0.21 m, which yields an aspect ratio (inner radius / thickness) of 20, subjected to an internal pressure of 19.294 MPa. At this pressure level, the plastic zone has just reached the outer radius of the tube. The exact analytical solution is described in Ref. [10].

Figure 3(top) presents the comparison for the axial stress distribution $\sigma_{xx}(r)$, Figure 3(middle) presents the comparison for the circumferential stress distribution $\sigma_{\theta\theta}(r)$, and Figure 3(bottom) presents the comparison for the radial stress distribution $\sigma_{rr}(r)$. In the case of the circumferential and radial stress distributions, the predictions of the higher-order theory differ from the exact analytical results by one or two percent. In the case of the axial stress distributions, somewhat higher differences are observed due to the very small magnitudes of the axial stress.

Figure 4 presents the axial (top), circumferential (middle), and radial (bottom) stress distributions predicted by the higher-order theory in a four-layer tube, composed of alternating Ti-24Al-11Nb and NiAl plies of equal thickness, and subjected to an internal pressure of 82.7 MPa. The innermost ply is composed of the titanium alloy, and the inner and outer radii of the tube are 25.4 mm and 30.5, respectively, yielding layer thickness of 1.3 mm. Included in the figure are the exact analytical predictions taken from Ref. [11]. Comparison of the higher-order theory predictions and exact results reveals that the axial and circumferential stress distributions are somewhat underestimated by the higher-order theory in the two middle layers and the titanium layers, respectively, while the radial stress distributions predicted by the two approaches are essentially the same. The differences can be explained by noting that the aspect ratio of the tube is very low (5) while the higher-order theory's framework is explicitly based on the assumption that the aspect ratio of a cylindrical component is high. The above comparison illustrates that the predictive capability of the theory can be quite good even for cylindrical components with relatively small aspect ratios. It should be noted, however, that the theory's accuracy will generally deteriorate with the cylindrical component's decreasing aspect ratio. This was ascertained in a parametric study using the data employed in the first example wherein the tube's thickness was increased to produce aspect ratios of 10 and 5.

The last set of results shown in Figure 5 presents the comparison between the predictions of **HOTCFGM-1D** and an exact analytical solution for the homogeneous tube of the first example subjected to an internal temperature of 1°C and outer temperature of 0°C. Virtually no differences are observed between the **HOTCFGM-1D** and exact results for the axial and circumferential stress distributions. Slightly worse correlation is observed for the radial stress distribution, which is most likely due to the small magnitudes of this stress component relative to the other components.

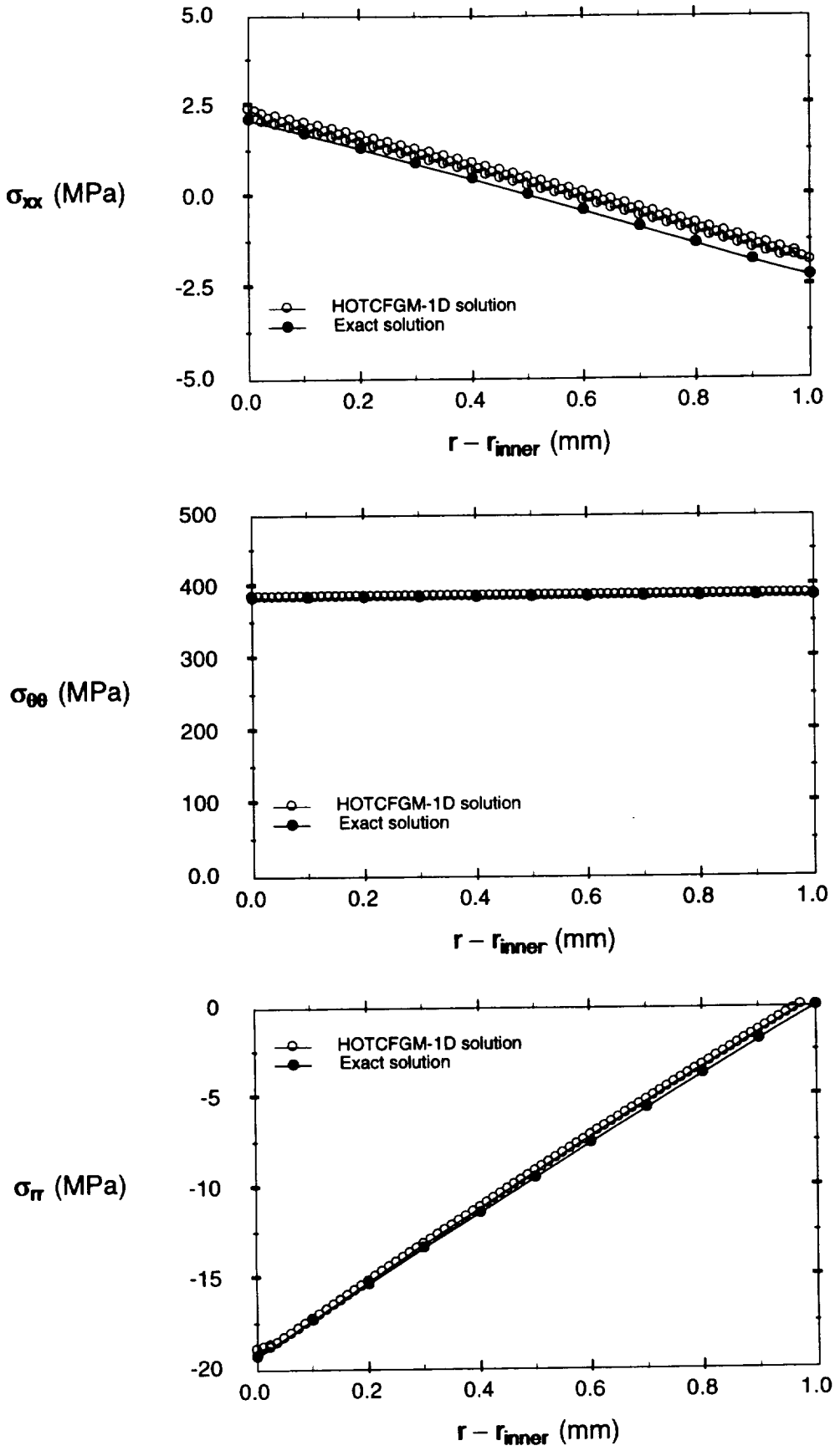

Figure 3. HOTCFGM-1D and exact solutions for a homogeneous elastoplastic tube subjected to internal pressure: axial (top); circumferential (middle); and radial stress (bottom) distributions.

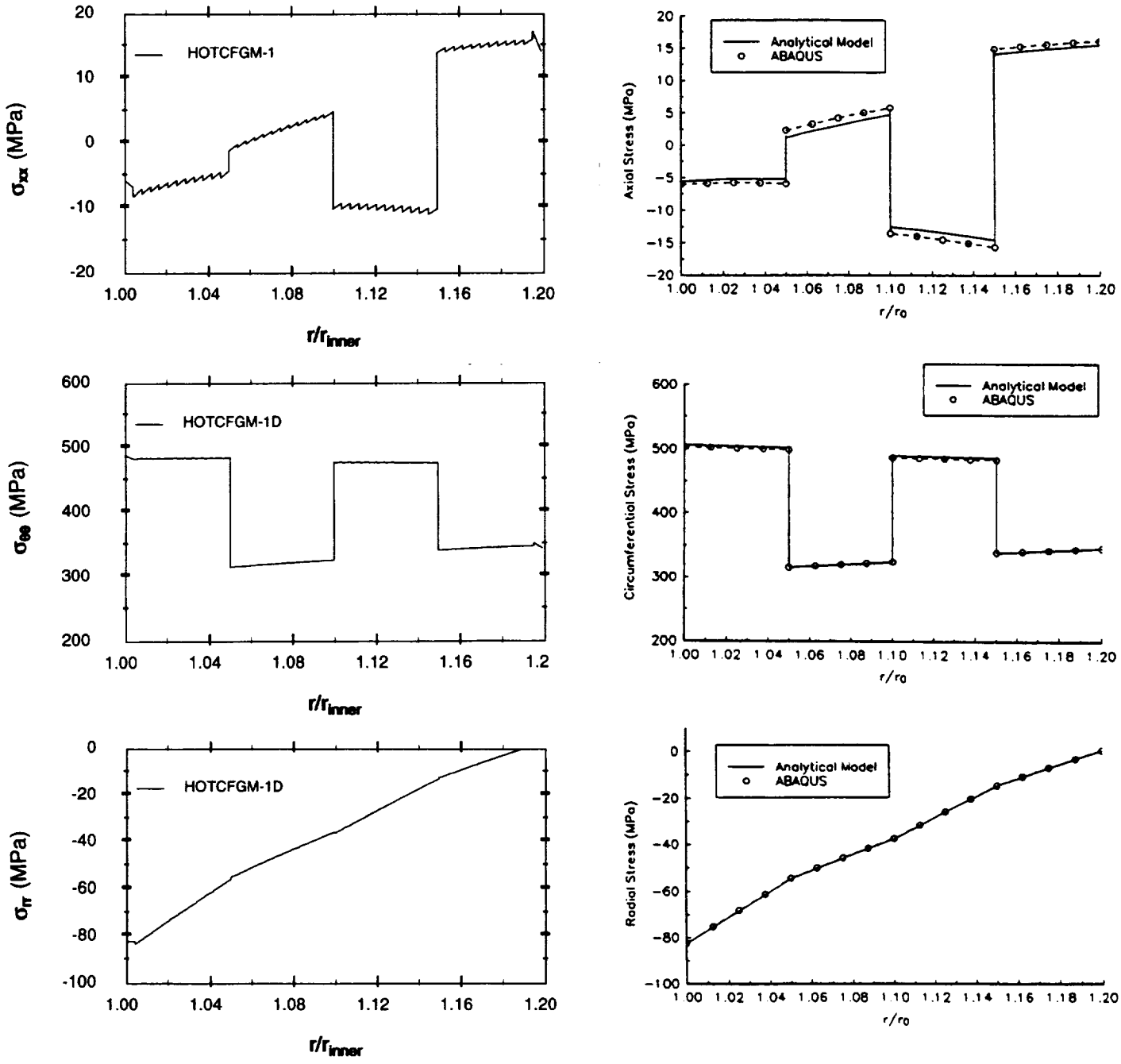

Figure 4. HOTCFGM-1D and exact solutions for a 4-layer elastoplastic tube subjected to internal pressure: axial (top); circumferential (middle); and radial stress (bottom) distributions.

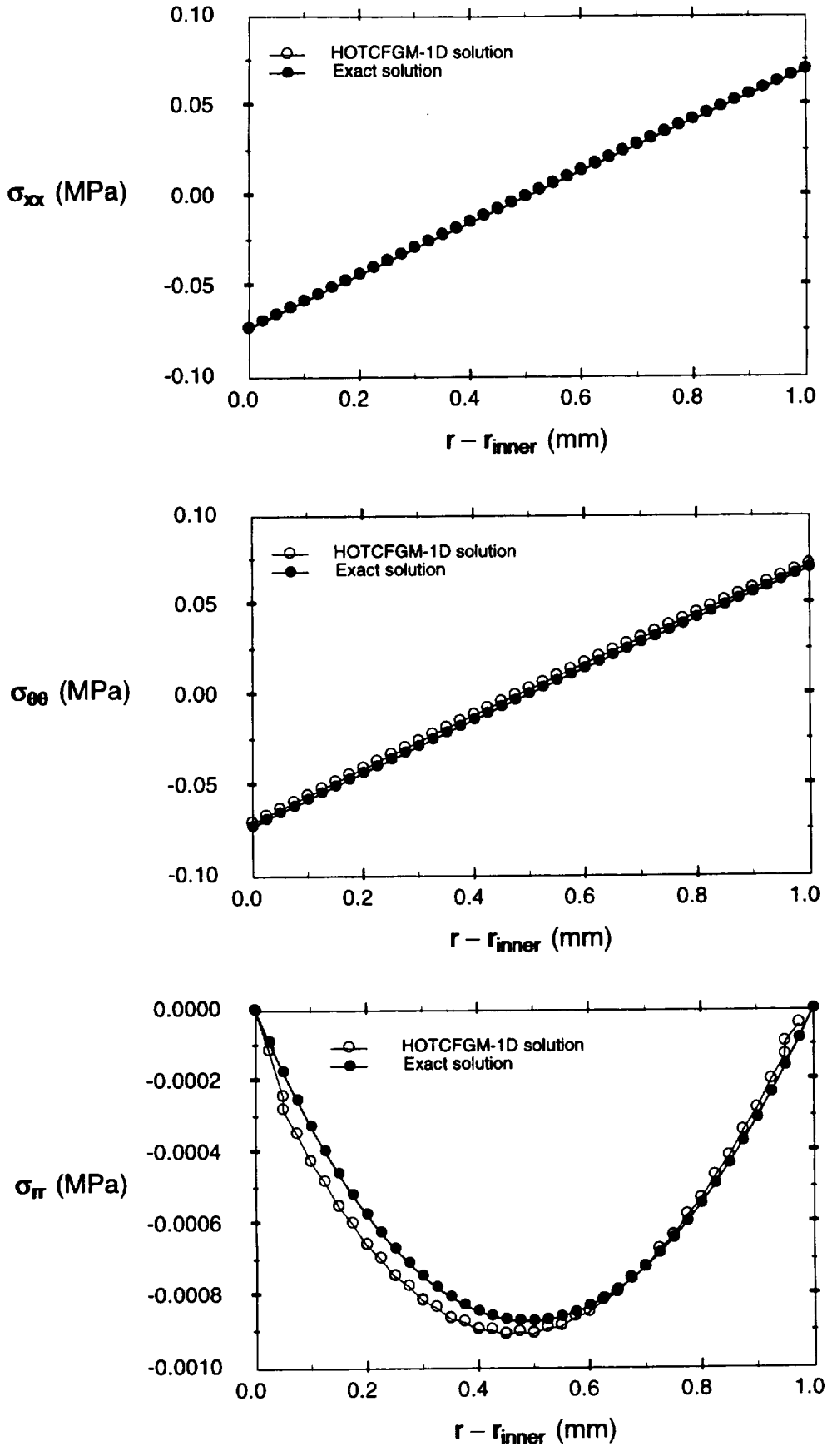

Figure 5. HOTCFGM-1D and exact solutions for a homogeneous tube subjected to a radial thermal gradient: axial (top); circumferential (middle); and radial stress (bottom) distributions.

4.2 Analysis of Microstructural Effects

In order to be able to compare the predictions of the higher-order theory with the commonly-used homogenization-based approaches in the analysis of functionally graded structural components, and thereby ascertain the importance of microstructural effects, the generalized method of cells (GMC) micromechanics model has been employed to develop the computer code *fgmp.homog.tube.f* for modeling functionally graded cylinders with heterogeneous phases. The micromechanics model, which is embedded within the theoretical framework of the higher-order theory, generates instantaneous effective properties of the heterogeneous phases used in the course of solving eqns (4) and (13). This capability also allows further validation of the higher-order theory, and also facilitates justification of its development. The homogenization-based capability of the computer code *fgmp.homog.tube.f* is demonstrated herein through two examples that illustrate the differences between the homogenization-based predictions and the predictions which explicitly take into account the actual microstructure of a heterogeneous cylinder. In the first example, a SiC/Ti tube subjected to an internal pressure is considered, whereas the same tube subjected to steady-state rotation is investigated in the second example.

4.2.1 SiC/Ti Tube Subjected to Internal Pressure

A SiC/Ti cylinder with an inner radius of 25.4 mm and an outer radius of 30.5 mm subjected to an internal pressure of 151.7 MPa was chosen for all the cases investigated. These dimensions yield an aspect ratio (inner radius / wall thickness) of 5. For the homogenization-based cases, as well as the cases involving explicit consideration of the cylinder's heterogeneity, the fiber volume fraction of the SiC fibers was fixed at 0.4.

To compare the homogenization-based results with the results that take into account the cylinder's actual heterogeneity, three cylindrical configurations reinforced by axially-oriented (0°) fibers were investigated as a function of the microstructural refinement. The coarsest configuration had four rows of fibers through the cylinder's thickness, while the intermediate and the finest configurations contained ten and twenty rows, respectively. Figures 6 through 9 illustrate the comparison between the homogenization-based and microstructure-based predictions generated by the computer codes *fgmp.homog.tube.f* and *fgmp.tube.f*, respectively, for the circumferential, radial, axial, and effective plastic strain distributions in the 0° cylinder subjected to the applied internal pressure. The microstructure-based results were generated in the fiber-matrix and matrix-matrix representative cross sections of the cylinder's microstructure.

As observed in the figures, the circumferential and axial stress distributions predicted by the microstructure-based analysis oscillate about the distributions based on the homogenized

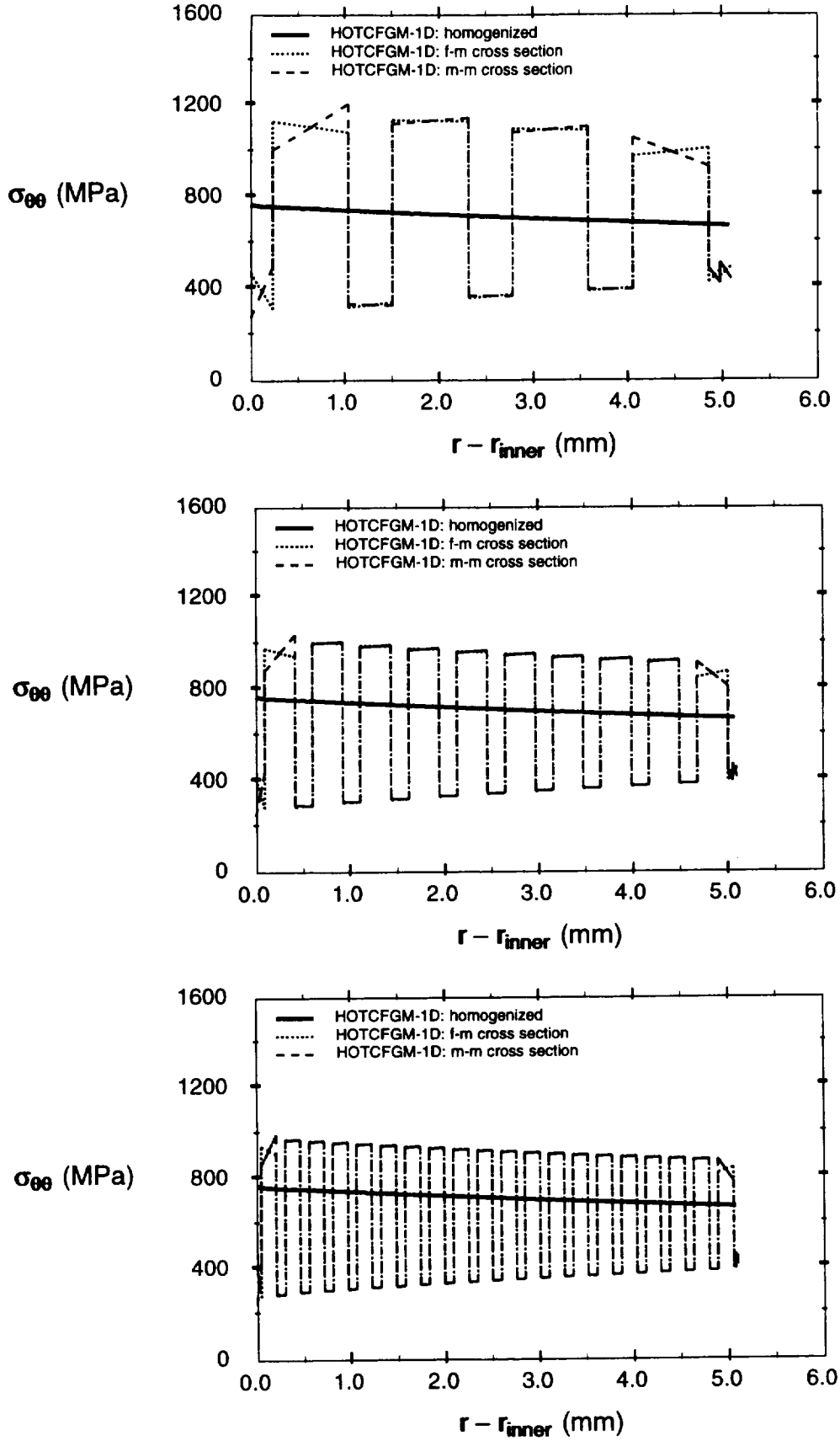

Figure 6. Through-thickness $\sigma_{\theta\theta}$ stress distributions in a 0° cylinder subjected to an internal pressure: 4-fiber row (top); 10-fiber row (middle); and 20-fiber row (bottom) configuration.

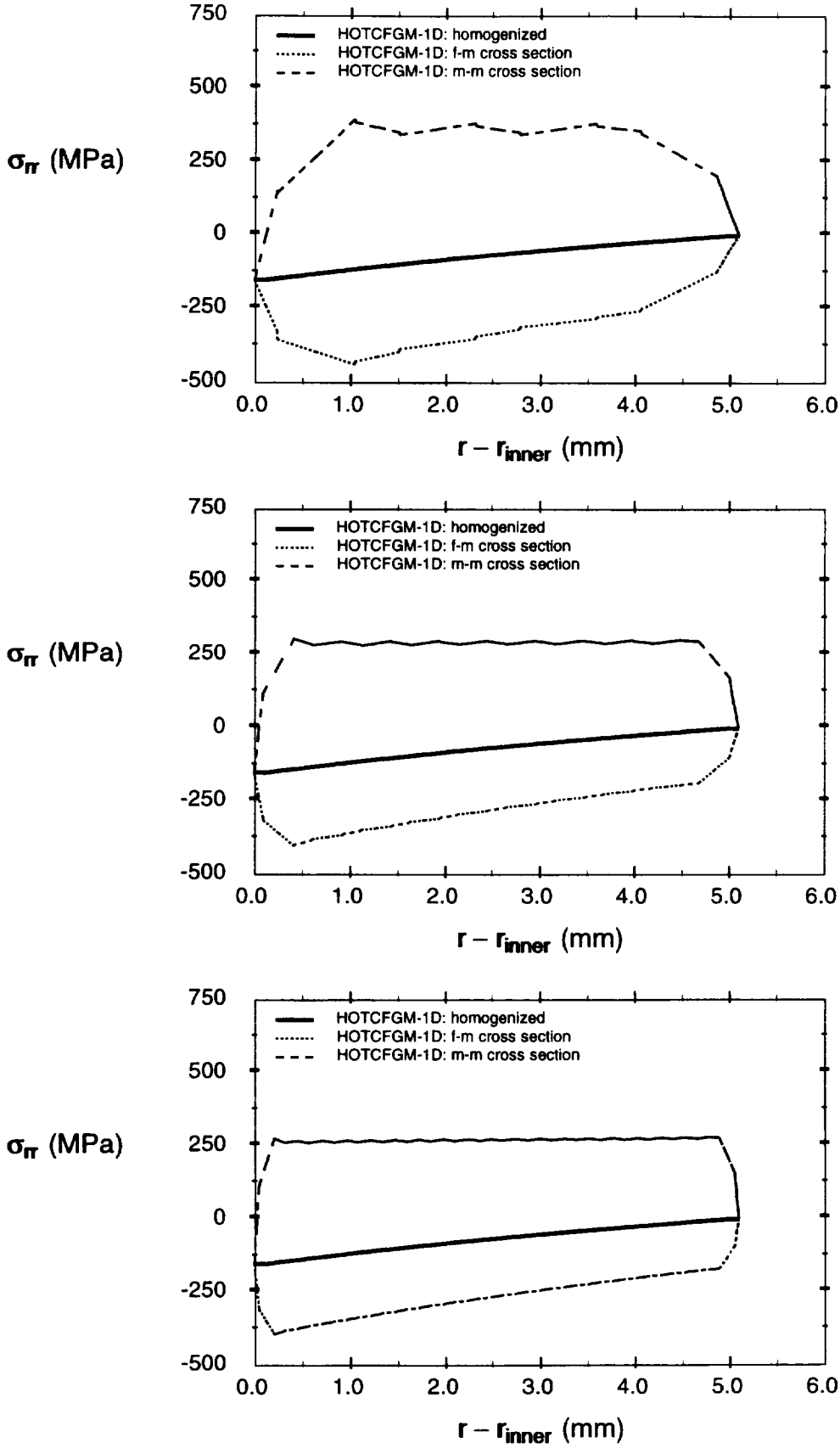

Figure 7. Through-thickness σ_{rr} stress distributions in a 0° cylinder subjected to an internal pressure: 4-fiber row (top); 10-fiber row (middle); and 20-fiber row (bottom) configuration.

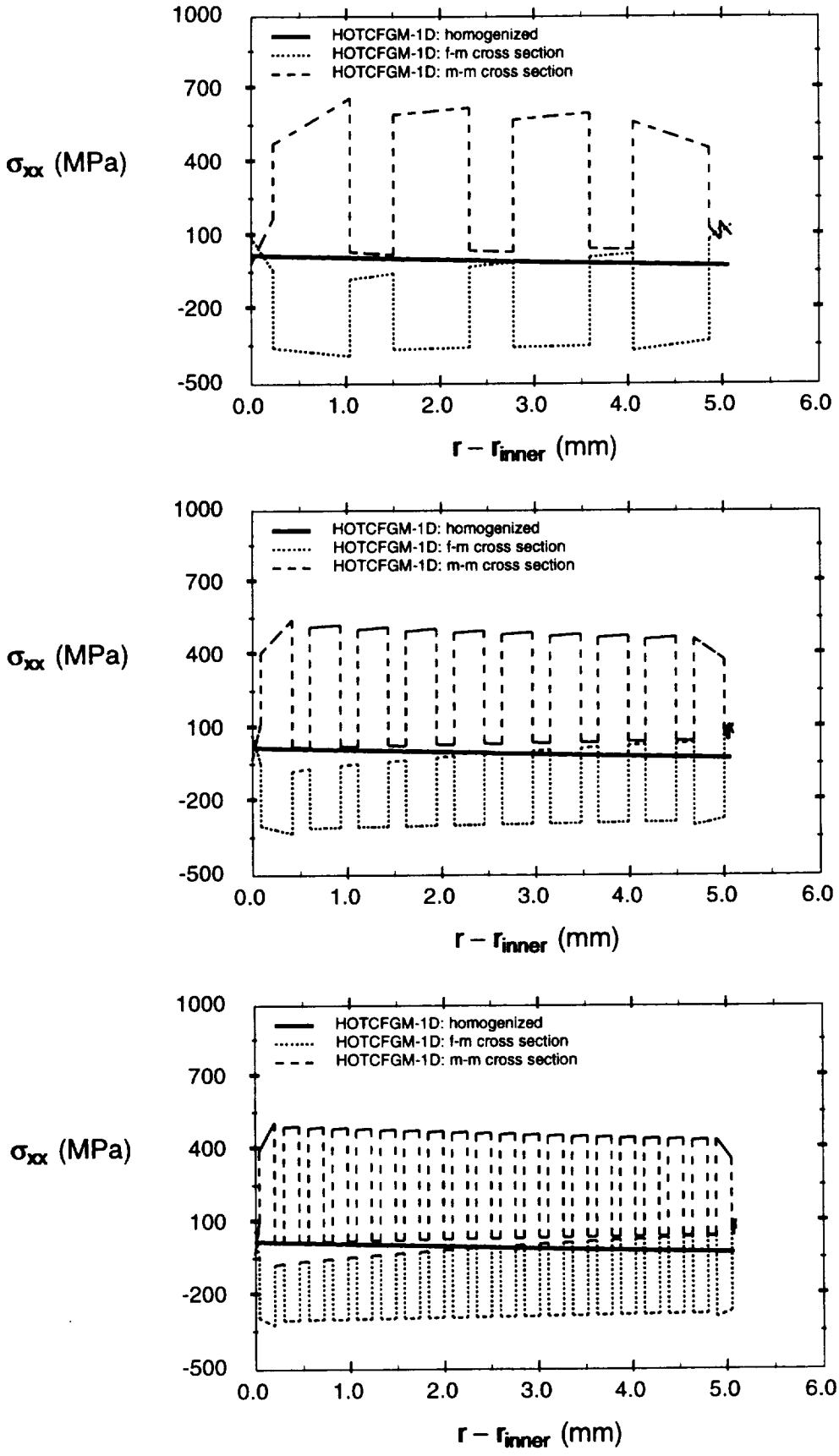

Figure 8. Through-thickness σ_{xx} stress distributions in a 0° cylinder subjected to an internal pressure: 4-fiber row (top); 10-fiber row (middle); and 20-fiber row (bottom) configuration.

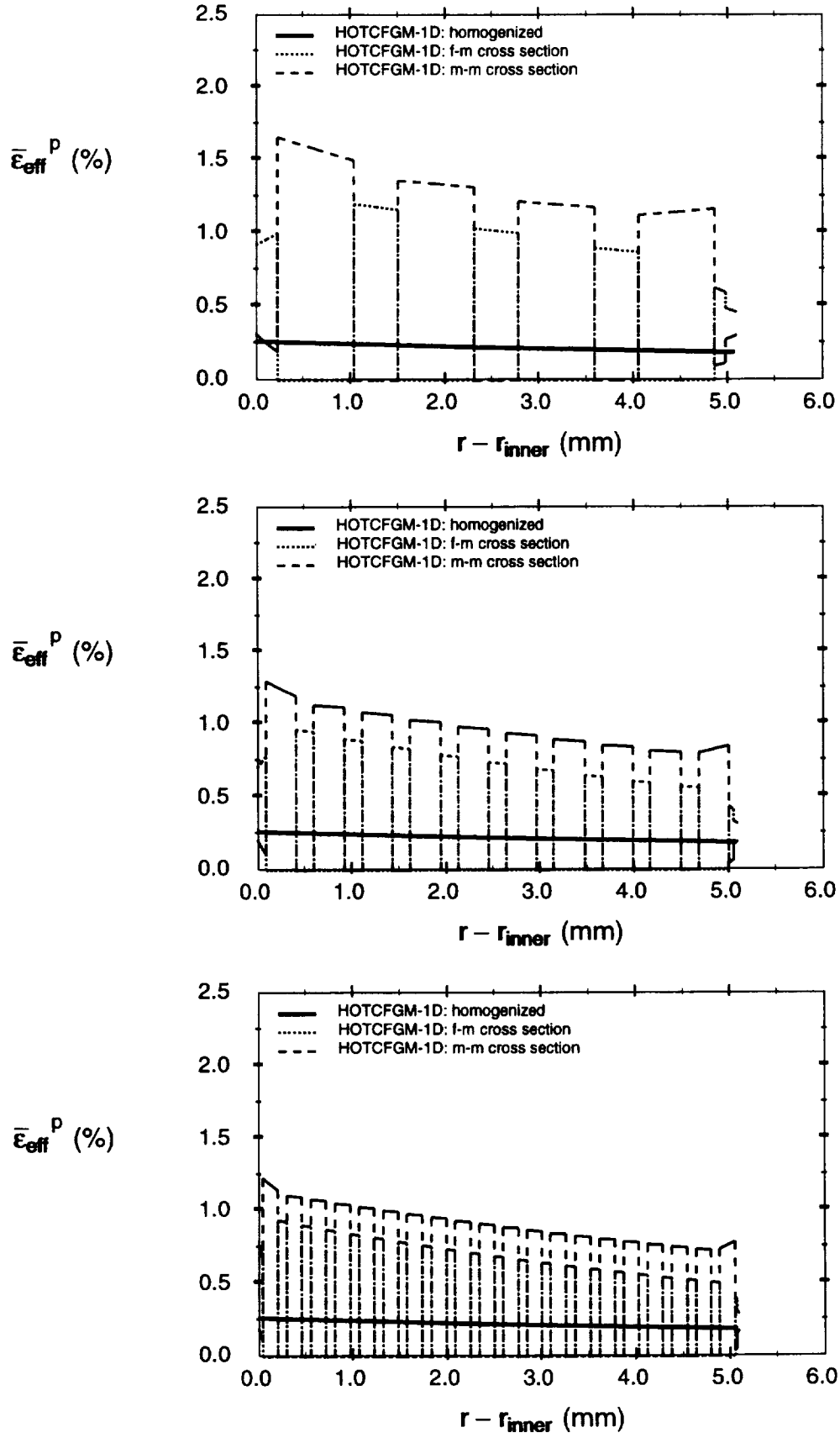

Figure 9. Through-thickness $\bar{\varepsilon}_{eff}^{p}$ plastic strain distributions in a 0° cylinder subjected to an internal pressure: 4-fiber row (top); 10-fiber row (middle); and 20-fiber row (bottom) configuration.

analysis (Figs. 6 and 8), the latter tending to provide average distributions. The amplitude of stress oscillations decreases with the microstructural refinement, i.e., the number of fiber rows through the cylinder's thickness, and reaches an asymptotic level for the configuration with twenty rows of fibers. Interestingly, the radial stress distributions predicted by the microstructure-based analysis, Fig. 7, become tensile in the matrix-matrix representative cross section in the cylinder's interior, while in the fiber-matrix cross section the expected compressive distributions are obtained. The deviation of the radial stress distributions from homogenization-based compressive distributions decreases with increasing microstructural refinement in both cross sections as in the preceding cases.

The amplitude of the oscillations in the effective plastic strain distributions predicted by the microstructure-based analysis also decreases with increasing microstructural refinement, reaching an asymptotic level for the configuration with twenty rows of fibers, Fig. 9. Unlike the stress distributions shown in Figs. 6 through 8, however, the homogenization-based effective plastic strain distributions are substantially smaller than the microstructure-based distributions, and thus do not appear to represent average distributions about which the latter predictions oscillate. This issue deserves further investigation.

4.2.2 SiC/Ti Tube Subjected to Steady-State Rotation

In this example, we focus on the effective plastic strain distributions induced by steady-state rotation in the three SiC/Ti configurations of the preceding section. The results will demonstrate that the effect of material's heterogeneity on the plastic strain fields depends on the type of applied loading, thereby further demonstrating the importance of the higher-order theory.

For each of the three configurations, a rotational velocity was determined which produced an effective plastic strain of 0.01% at the outer radius of the tube. This rotational velocity results in full plastification of the entire cross section of the tube. The corresponding rotation velocity based on the homogenization scheme was also determined. The rotational velocities necessary to produce full plastification of the heterogeneous configurations normalized by the corresponding rotational velocity for the homogenized tube were determined to be: $\omega/\omega_{homogenized} = 1.07$, 1.11, and 1.12 for the 4-fiber, 10-fiber, and 20-fiber configurations, respectively.

Figure 10 illustrates the effective plastic strain distributions in the fiber-matrix cross sections of the three configurations. In contrast with the preceding results involving the application of internal pressure, the present results indicate that the magnitude of the plastic strain field oscillations increases with increasing microstructural refinement. As in the preceding case, the magnitude of the plastic strain field predicted by the homogenization-based approach is substantially underestimated relative to the higher-order theory predictions.

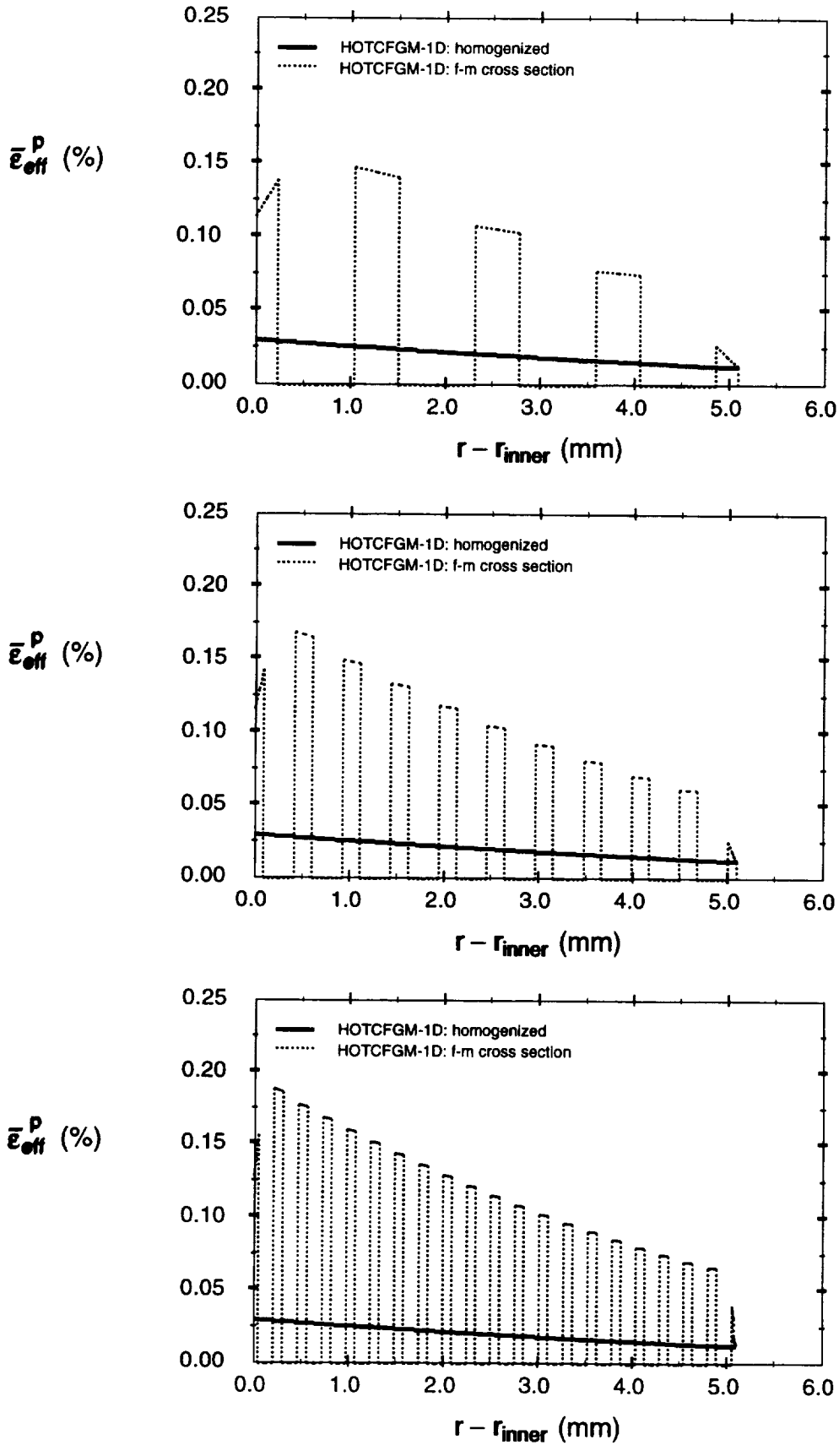

Figure 10. Through-thickness $\bar{\varepsilon}^p_{eff}$ plastic strain distributions in a 0° cylinder under steady-state rotation: 4-fiber row (top); 10-fiber row (middle); and 20-fiber row (bottom) configuration.

4.3 Optimization Studies

To demonstrate the optimization capability of the computer code *fgmp.tube.opt.f*, two examples are presented involving the previously considered 0° SiC/Ti tubes subjected to internal pressure and steady-state rotation. The design variables were the fiber spacings in the through-thickness direction subject to the constraint that the minimum spacings be greater than one fourth and one eighth of the fiber diameter in the interior and at the exterior boundaries, respectively. Configurations with four and ten rows of fibers through the cylinder's thickness were considered, with the initial designs having uniform fiber spacing as in the preceding cases. In the first example involving internal pressurization, the optimization capability is demonstrated for elastic phases, while in the second example elastoplastic phases are considered.

4.3.1 Optimization of SiC/Ti Tubes Under Internal Pressure

In this example, the objective function to be minimized was the moment produced by the circumferential stress component induced by the applied internal pressure in the two configurations. This objective function was coded into the computer program *fgmp.tube.opt.f* which was subsequently recompiled to create an executable file with the chosen objective function. In the future, the objective function will be located in an appropriate subroutine that will contain a selection of commonly-used objective functions, including a user-defined function.

The results of the optimization studies are presented in Table 4 and 5 where the initial and optimum designs and the resulting moments are shown for the two configurations. The first and last fiber spacings given in the tables refer to the distances between the innermost and outermost fibers and the inner and outer radii, respectively, while the remaining spacings are the fiber-to-fiber spacings in the cylinder's interior. As observed, dramatic reductions in the moment produced by the circumferential stress component can be achieved by biasing the fiber locations toward the outer radius of the cylinder. Figures 11 and 12 illustrate the initial and optimum circumferential stress distributions in the two configurations.

Table 4. Initial and optimum designs for the 4-fiber configuration.

Design	Moment	Fiber spacing distances (mm)				
Initial	-309.9	0.234	0.469	0.469	0.469	0.234
Optimum	-0.46	0.414	0.570	0.453	0.336	0.100

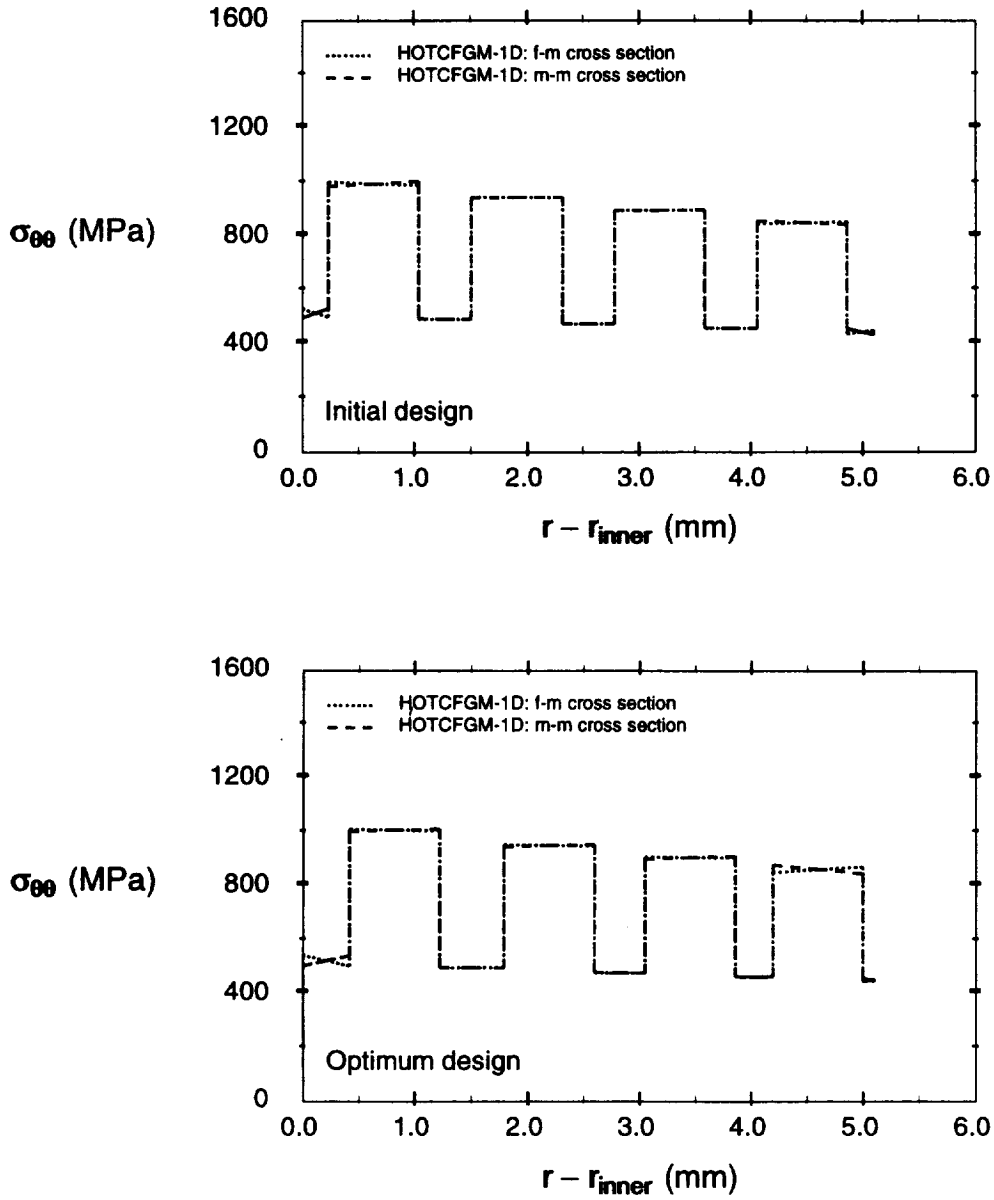

Figure 11. Initial (top) and optimum (bottom) through-thickness $\sigma_{\theta\theta}$ stress distributions in a 0°, 4-fiber row cylinder subjected to an internal pressure of 151.7 MPa.

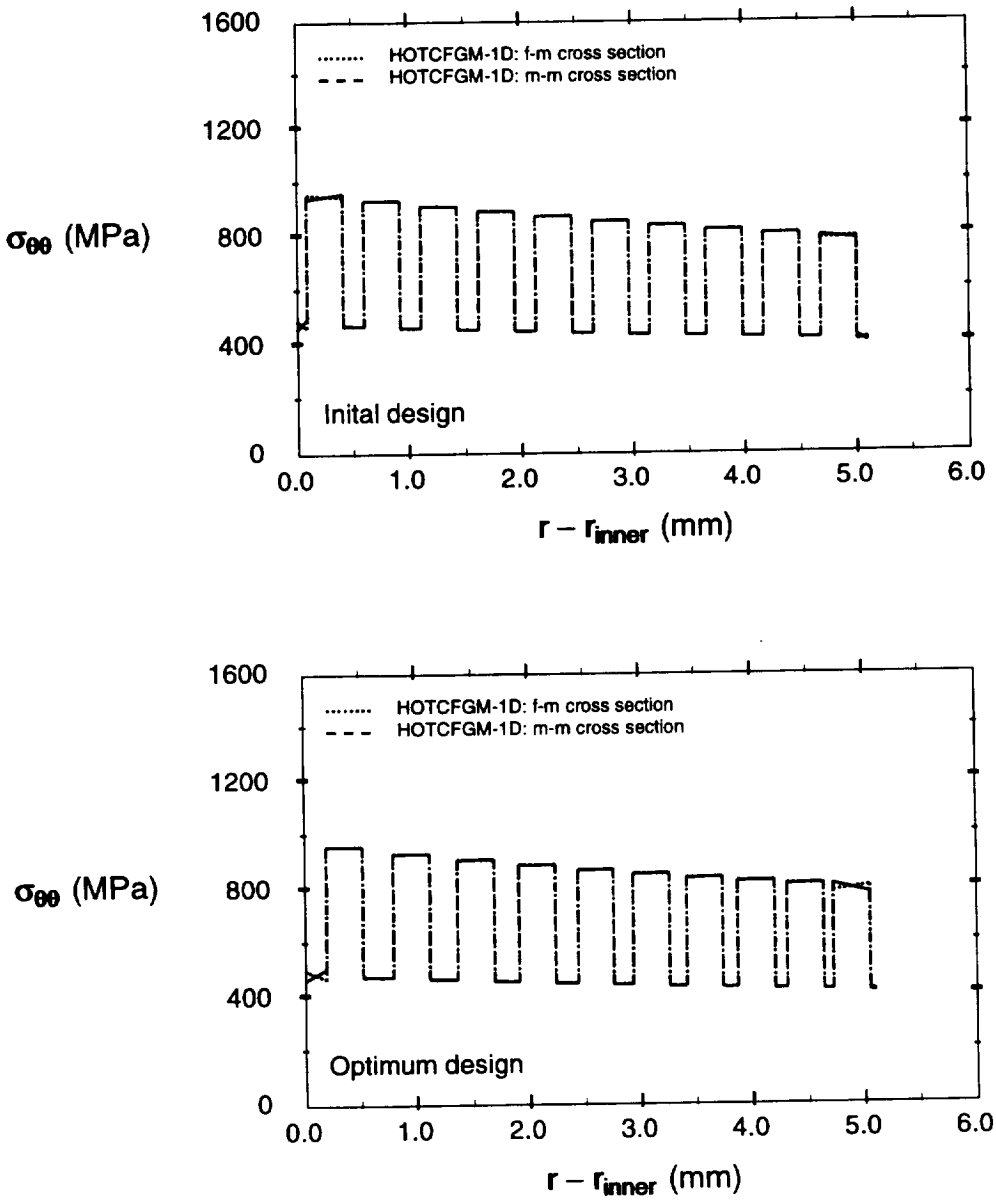

Figure 12. Initial (top) and optimum (bottom) through-thickness $\sigma_{\theta\theta}$ stress distributions in a 0°, 10-fiber row cylinder subjected to an internal pressure of 151.7 MPa.

Table 5. Initial and optimum designs for the 10-fiber configuration.

Design	Moment	Fiber spacing distances (mm)									
Initial	-300.0	0.093	0.186	0.186	0.186	0.186	0.186	0.186	0.186	0.186	0.093
Optimum	3.2	0.199	0.274	0.246	0.221	0.197	0.175	0.155	0.135	0.113	0.088	0.047

4.3.2 Optimization of Rotating SiC/Ti Tubes

In this example, the objective function to be minimized was the total accummulated effective plastic strain produced by the steady-state rotation in the outer third of the two configurations. This objective function was again coded into the computer program *fgmp.tube.opt.f* which was subsequently recompiled to create an executable file with the new objective function.

The optimization results are presented in Table 6 and 7 where the initial and optimum designs and the resulting total accummulated plastic strains in the outer third of each configurations are given. Similar to the preceding cases involving internal pressurization, substantial (but not as dramatic) reductions in the accummulated plastic strain in the outer third of each configuration produced by the steady-state rotation are achieved. In contrast with the preceding case, however, this is accomplished by biasing the fiber locations toward the cylinder's inner radius.

Table 6. Initial and optimum designs for the 4-fiber configuration.

Design	$\bar{\varepsilon}^{p}_{eff}$	Fiber spacing distances (mm)				
Initial	1.10%	0.234	0.469	0.469	0.469	0.234
Optimum	0.48%	0.100	0.200	0.200	0.850	0.520

Table 7. Initial and optimum designs for the 10-fiber configuration.

Design	$\bar{\varepsilon}^{p}_{eff}$	Fiber spacing distances (mm)									
Initial	2.26%	0.093	0.186	0.186	0.186	0.186	0.186	0.186	0.186	0.186	0.093
Optimum	1.37%	0.041	0.081	0.081	0.081	0.081	0.081	0.081	0.576	0.343	0.081	0.326

Figure 13 llustrates the optimum effective plastic strain distributions in the two configurations that can be compared with the corresponding ones in Fig. 10 for the uniformly spaced configurations. The results indicate that in addition to the reduction in the total accumulated plastic strain in the outer third of the cylinders' cross sections, the optimum fiber distributions dramatically reduce the plastic strain directly at the outer radius. Further refinement of the optimum fiber spacings can be obtained by employing the optimum fiber spacings obtained herein as initial design variables in a second iteration of the optimization procedure. This should eliminate the plastic strain spike in the 10-fiber configuration in the region immediately adjacent to the outermost fiber observed in the figure.

5.0 PLANS FOR FUTURE WORK

The second year of the project involves generalization of the quasi one-dimensional version of the higher-order theory to two dimensions, as outlined in Ref. [12]. This version will enable the analysis and design of cylindrical structural components functionally graded in two directions in the cylinder's cross section. This version will also make possible the analysis of finite cylindrical bodies of revolution, in addition to complete bodies of revolution, thereby allowing consideration of such aircraft engine structural components as turbine blades.

In addition, work will continue on the development of more user-friendly versions of the current computer programs, application of these programs to technologically important problems such as functionally graded combustor linings and thermal barrier coatings, as well as incorporation of robust integration algorithms, upon their availability, for use with the GVIPS model as outlined in Refs. [13,14].

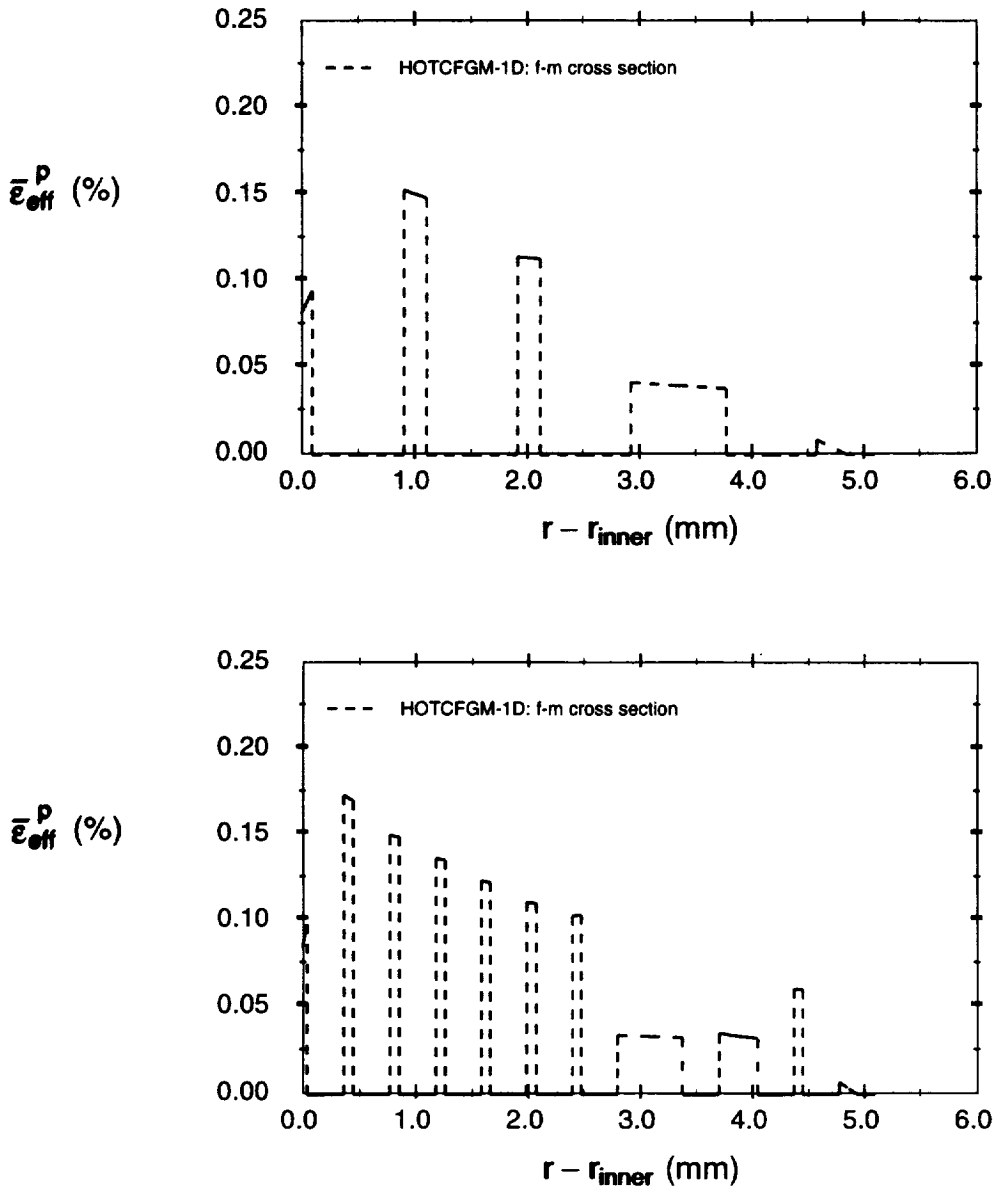

Figure 13. Optimum through-thickness $\bar{\varepsilon}^p_{eff}$ plastic strain distributions in a 0° cylinder under steady-state rotation: 4-fiber row (top); and 10-fiber row (bottom).

6.0 REFERENCES

1. Mendelson, A., *Plasticity: Theory and Applications*, Robert E. Krieger Publishing Company, Malabar, Florida, 1983 (reprint edition).
2. Arnold, S. M., Saleeb, A. F., and Castelli, M. G. (1994), "A Fully Associative, Nonlinear Kinematic, Unified Viscoplastic Model for Titanium Based Matrices," *NASA TM 106609*, NASA-Lewis Research Center, Cleveland, OH.
3. *DOT User's Manual, Version 4.00.* (1993), VMA Engineering, Vanderplaats, Miura & Associates, Inc., Goleta, CA.
4. Pindera, M-J. and Aboudi, J., "HOTFGM-Cylinder: A Coupled Micro-Macrostructural Theory for the Response of Cylindrical Functionally Graded Structural Components - A Proposal in Response to NRA-96-LeRC-1," *SEAS Proposal No. CEAM-NASA/LeRC-7029-96*, School of Engineering & Applied Science, University of Virginia, February 1996.
5. Vanderplaats, G. N., *Numerical Optimization Techniques for Engineering Design With Applications*, McGraw-Hill, New York, 1984.
6. Aboudi, J., *Mechanics of Composite Materials: A Unified Micromechanical Approach*, Elsevier, The Netherlands, 1991.
7. Aboudi, J., Pindera, M-J., and Arnold, S. M., "Higher-Order Theory for Axisymmetric Analysis of Cylindrical Functionally Graded Structural Components", (in preparation).
8. Aboudi, J., Pindera, M-J., and Arnold, S. M., "Optimization of Cylindrical Functionally Graded Structural Components Using the Coupled Higher-Order Theory", to be presented at ICCE/5, July 5-11, 1998, Las Vegas, NV.
9. Pindera, M-J., Aboudi, J., and Arnold, S. M., "Analysis of Microstructural Effects in Cylindrical Functionally Graded Structural Components Using the Coupled Higher-Order Theory", to be presented at FGM'98, October 26-29, 1998, Dresden, Germany.
10. Salzar, R. S., Pindera, M-J., and Barton, F. W., "Elastic/Plastic Analysis of Layered Metal Matrix Composite Cylinders. Part I: Theory," *Journal of Pressure Vessel Technology*, Vol. 118, No. 1, 1996, pp. 13-20.
11. Salzar, R. S., Pindera, M-J., and Barton, F. W., "Elastic/Plastic Analysis of Layered Metal Matrix Composite Cylinders. Part II: Applications," *Journal of*

Pressure Vessel Technology, Vol. 118, No. 1, 1996, pp. 21-26.

12. Pindera, M-J. and Aboudi, J., "HOTFGM-Cylinder: A Coupled Micro-Macrostructural Theory for the Response of Cylindrical Functionally Graded Structural Components - A Proposal in Response to NRA-97-LeRC-2," *SEAS Proposal No. CEAM-NASA/LeRC-7431-97*, School of Engineering & Applied Science, University of Virginia, February 1997.

13. Saleeb, A. F. and Li, W. (1995a), "Robust Integration Schemes for Generalized Viscoplasticity with Internal-State Variables. Part I: Theoretical Developments and Applications," *NASA CR 195452*, NASA-Lewis Research Center, Cleveland, OH.

14. Saleeb, A. F. and Li, W. (1995b), "Robust Integration Schemes for Generalized Viscoplasticity with Internal-State Variables. Part II: Algorithmic Developments and Implementation" *NASA CR 195453*, NASA-Lewis Research Center, Cleveland, OH.

7.0 APPENDICES

7.1 Appendix 1

The input data file *fgmp.tube.data* is organized into four distinct blocks, as explained in section 3.1. The structure of the input data file, the variable names and their description read by the program are given below.

Block 1: Material properties for NMT materials at NTEMP identical temperatures

NMAT	number of materials
	begin sequential specification of different materials --> repeat NMAT times
MNAME	material name
ID	material identification number (1, 2, . . . , NMAT)
NTEMP	Number or temperatures at which material properties are specified
	begin sequential material property input at a given temperature --> repeat NTEMP times
IT1, TEMP	temperature number (1, 2, . . . , NTEMP), temperature at which material properties are specified
CONDATEMP,CONDTTEMP	axial and transverse thermal conductivities at TEMP
EATEMP,ETTEMP,GATEMP	axial and transverse Young's moduli, and axial shear modulus at TEMP
FNATEMP,FNTTEMP	axial and transverse Poisson's ratios at TEMP
ALPATEMP,ALPTTEMP	axial and transverse thermal expansion coefficients at TEMP
YIELDTEMP,HARDTEMP	yield stress and hardening slope at TEMP
	end of material property input at a given temperature
	end of material property input for NMAT materials at NTEMP temperatures

Note: HARDTEMP *is obtained from a uniaxial stress-strain curve at a given temperature. It is defined as:* HARDTEMP = $d\sigma/d\varepsilon^p = m*E/(E-m)$ *where* $m = d\sigma/d\varepsilon$

Block 2: Loading specification and write options

TREF	reference temperature
AMPTOPT,AMPBOTT	maximum temperatures applied at the top and bottom surfaces
LOADTOPM,LOADBOTM	mechanical loading type indicators for top and bottom surfaces: 1 -> radial traction; 2 -> radial displacement
AMPTOPM,AMPBOTM	maximum values of mechanical loading (radial traction/displacement)
ISW,FLOAD	axial constraint indicator, magnitude of axial load: ISW=1 -> average axial strain imposed; ISW=2 -> average axial stress imposed
OMEGAF	magnitude of steady-state angular velocity
NINT,NINA	total number of load increments used in the solution of equations (4) and (13) -> defines load increment size; actual number of load increments
MAXITERATION	number of iterations used in the solution of equation (13) at each load increment
NSTEP	number of load increments between which output data is written to the *fgmp.tube.out* file
NPLOT1,NPLOT2,NPLOT3,NPLOT4	specification of the four increments at which output results are written to the *fgmp.tube.plot* file
JPLOT,KPLOT	specification of the subcells β, γ through which output results are written to the *fgmp.tube.plot* file

Block 3: Specification of the cylinder architecture and geometry

M	number of cells in the radial direction
	begin subcell dimensions specifications --> repeat M times
NCELL,D1,D2	cell number, subcell dimensions $d_1^{(p)}$ and $d_2^{(p)}$
	end of subcell dimensions specifications for M cells
NTHETA,H1H2,R0	number of cells along the θ-direction, ratio of the subcell dimensions h_1/h_2, inner radius of the cylinder
L1,L2	subcell dimensions l_1 and l_2
	begin subcell material assignment --> repeat M times
NCELL1,MATNUM	cell number, material assignment in the eight subcells (1 1 1) --> (2 2 2) of each cell
	end of subcell material assignment for M cells

Block 4: Specification of the approximation of integration of the plastic strain field in the individual subcells in equation (13)

NLEG1,NLEG2,NLEG3	order of Legendre polynomials in the radial, angular and axial direction
J1,J2,J3	number of integration points in the radial, angular and axial directions

7.2 Appendix 2

The input file *fgmp.tube.data* for the case described in section 4.2.2 is given below. The highlighted text, not to be included in the input deck, identifies the four blocks of the input data.

Block 1

```
2                                                    NMAT
SiC                                                  MNAME
1                                                    ID
1                                                    NTEMP
1     0.0E+00                                        IT1,TEMP
8.0   8.0                                            CONDATEMP,CONDTTEMP
399.90E+09    399.90E+09   159.96E+09                EATEMP,ETTEMP,GATEMP
  0.25E+00      0.25E+00                             FNATEMP,FNTTEMP
  1.00E-06      1.00E-06                             ALPATEMP,ALPTTEMP
  0.00E+06     23.00E+09                             YIELDTEMP,HARDTEMP

Ti
1
1
1     0.0E+00
8.0           8.0
110.30E+09    110.30E+09    43.77E+09
0.26E+00      0.26E+00
1.00E-06      1.00E-06
71.60E+06     23.00E+09
```

Block 2

```
0                                                    TREF
0         0                                          AMPTOPT,AMPBOTT
1         1                                          LOADTOPM,LOADBOTM
0         0.                                         AMPTOPM,AMPBOTM
2         0.                                         ISW,FLOAD
7700E2                                               OMEGAF
100       100                                        NINT,NINA
10                                                   MAXITERATION
25                                                   NSTEP
1     100     10000   10000                          NPLOT1,NPLOT2,NPLOT3,NPLOT4
1     1                                              JPLOT,KPLOT
```

Block 3

```
5                                                    M
1          0.2344E-3          0.8062E-3              NCELL,D1,D2
2          0.4688E-3          0.8062E-3              .
3          0.4688E-3          0.8062E-3              .
4          0.4688E-3          0.8062E-3              .
5          0.2344E-3          0.1000E-8              .
125        1.72              25.4E-3                 NTHETA,H1H2,R0
0.8062E-3     0.4688E-3                              L1,L2
1      2 2 2 2 1 1 2 2                               NCELL1,MATNUM(1,1,1)...MATNUM(2,2,2)
2      2 2 2 2 1 1 2 2                               .
3      2 2 2 2 1 1 2 2                               .
4      2 2 2 2 1 1 2 2                               .
5      2 2 2 2 1 1 1 1                               .
```

Block 4

```
2  2  2                                              NLEG1,NLEG2,NLEG3
5  5  5                                              J1,J2,J3
```

7.3 Appendix 3

The output file *fgmp.tube.out* generated by the input file *fgmp.tube.data* of the preceding section is given below.

```
**************************************************
**      FUNCTIONALLY GRADED CYLINDRICAL TUBE      **
**                                                **
**       IN THE RADIAL (THICKNESS) DIRECTION      **
**                                                **
**     DETERMINATION OF THE BEHAVIOR OF ELASTIC   **
**     AND ELASTOPLASTIC RESPONSE OF TEPERATURE-  **
**       DEPENDENT MULTI-PHASE FG TUBE            **
**                                                **
**                  PROGRAMMED BY                 **
**                  JACOB ABOUDI                  **
**                    MAY 1996                    **
**************************************************

************** INPUT DATA ECHO **************

             MATERIAL SPECIFICATION

NUMBER OF MATERIALS (NMAT) =  2

                     MATERIAL 1

AXIS OF SYMMETRY OF THE TRANSVERSELY ISOTROPIC MATERIAL IS : 1
NUMBER OF DIFFERENT TEMPERATURES (NTEMP)=  1

           TEMPR. # = 1          TEMPR. = 0.000E+00

 THERMAL CONDUCTIVITIES

KA    =  0.800E+01     KT    =  0.800E+01

 THERMO-ELASTIC CONSTANTS

EA    =  0.400E+12     ET    =  0.400E+12     GA =  0.160E+12
NUA   =  0.250E+00     NUT   =  0.250E+00
ALFA  =  0.100E-05     ALFT  =  0.100E-05

 INELASTIC PARAMETERS

YIELD    =  0.000E+00      HARDENING    =  0.230E+11

                     MATERIAL 2

AXIS OF SYMMETRY OF THE TRANSVERSELY ISOTROPIC MATERIAL IS : 1
NUMBER OF DIFFERENT TEMPERATURES (NTEMP)=  1

           TEMPR. # = 1          TEMPR. = 0.000E+00

 THERMAL CONDUCTIVITIES

KA    =  0.800E+01     KT    =  0.800E+01

 THERMO-ELASTIC CONSTANTS

EA    =  0.110E+12     ET    =  0.110E+12     GA =  0.438E+11
NUA   =  0.260E+00     NUT   =  0.260E+00
ALFA  =  0.100E-05     ALFT  =  0.100E-05
```

```
 INELASTIC PARAMETERS

YIELD    =  0.372E+09      HARDENING    =  0.230E+11

                LOADING SPECIFICATION

THE REFERENCE TEMPERATURE =  0.000E+00

APPLIED TEMPERATURE DEVIATION FROM TREF. AT THE OUTER SURFACE =  0.000E+00
APPLIED TEMPERATURE DEVIATION FROM TREF. AT THE INNER SURFACE =  0.000E+00

TYPES OF MECHANICAL LOADING AT THE OUTER AND INNER SURFACES : 1 AND 1
AMPLITUDES OF MECHANICAL LOADING AT THE OUTER AND INNER SURFACES : 0.000E+00 0.000E+00

IMPOSE SIGMAB33 =   0.000E+00

FINAL ROTATIONAL VELOCITY = OMEGAF =   0.770E+06

NUMBER OF INTEGRATION INCREMENTS =    100
ACTUAL NUMBER OF INCREMENTS =    100
MAX. NO. OF MENDELSON SUCCESSIVE ITERATIONS =  10

NUMBER OF PRINT STEPS OF THE  FIELD =   25
RESULTS ARE PLOTTED AT THE FOLLOWING 4 INCREMENTS :
        1      100    10000    10000

PLOTTING THROUGH SUBCELLS : J=1  K=1

                GEOMETRY  SPECIFICATION

NUMBER OF CELLS IN THE X-1 DIRECTION =    5

CELL # =  1     D1 =  0.234E-03     D2 =  0.806E-03
CELL # =  2     D1 =  0.469E-03     D2 =  0.806E-03
CELL # =  3     D1 =  0.469E-03     D2 =  0.806E-03
CELL # =  4     D1 =  0.469E-03     D2 =  0.806E-03
CELL # =  5     D1 =  0.234E-03     D2 =  0.100E-08

NO. OF CELLS IN THE THETA DIRECTION = NTHETA = 125

H1 / H2 =   0.172E+01

TUBE INNER RADIUS = R0 =   0.254E-01

L1 =   0.806E-03       L2 =   0.469E-03

                SUBCELL MATERIAL ASSIGNMENT

CELL # = 1          2  2  2  2  1  1  2  2
CELL # = 2          2  2  2  2  1  1  2  2
CELL # = 3          2  2  2  2  1  1  2  2
CELL # = 4          2  2  2  2  1  1  2  2
CELL # = 5          2  2  2  2  1  1  1  1

ORDER OF LEGENDRE POLYNOME =  2  2  2
NUMBER OF INTEGRATION POINTS =  5  5  5


**************** OUTPUT ******************

          TOTAL NO. OF CELLS = M = 5

     TOTAL THICKNESS IN X1-DIRECTION= 0.510E-02
     R0 / THICKNESS = 0.498E+01
```

```
   THETA1(deg) =   0.182E+01     THETA2(deg) =   0.106E+01

 NCELL=  1      D1= 0.234E-03     D2= 0.806E-03     D1+D2= 0.104E-02
                H1= 0.811E-03     H2= 0.472E-03     H1+H2= 0.128E-02

 NCELL=  2      D1= 0.469E-03     D2= 0.806E-03     D1+D2= 0.128E-02
                H1= 0.848E-03     H2= 0.493E-03     H1+H2= 0.134E-02

 NCELL=  3      D1= 0.469E-03     D2= 0.806E-03     D1+D2= 0.128E-02
                H1= 0.888E-03     H2= 0.517E-03     H1+H2= 0.140E-02

 NCELL=  4      D1= 0.469E-03     D2= 0.806E-03     D1+D2= 0.128E-02
                H1= 0.929E-03     H2= 0.540E-03     H1+H2= 0.147E-02

 NCELL=  5      D1= 0.234E-03     D2= 0.100E-08     D1+D2= 0.234E-03
                H1= 0.966E-03     H2= 0.561E-03     H1+H2= 0.153E-02

                L1= 0.806E-03     L2= 0.469E-03     L1+L2= 0.128E-02


       MATERIAL # = 1       VOLUME RATIO =  0.400E+00
       MATERIAL # = 2       VOLUME RATIO =  0.600E+00


            INCREMENT=   1

NCELL= 1  NSUB=1  (1,1,1)   JJ1= 1  X1= 0.000E+00
          TEMP= 0.000E+00   EPS  = -0.967E-07  0.333E-06 -0.574E-07
                            EPSP =  0.000E+00  0.000E+00  0.000E+00  0.000E+00  0.000E+00
                            SIGMA= -0.313E-04  0.376E+05  0.344E+04  0.330E+04 -0.873E+02

NCELL= 1  NSUB=1  (1,1,1)   JJ1= 3  X1= 0.117E-03
          TEMP= 0.000E+00   EPS  = -0.109E-06  0.331E-06 -0.574E-07
                            EPSP =  0.000E+00  0.000E+00  0.000E+00  0.000E+00  0.000E+00
                            SIGMA= -0.181E+04  0.367E+05  0.274E+04  0.330E+04 -0.873E+02

NCELL= 1  NSUB=1  (1,1,1)   JJ1= 5  X1= 0.234E-03
          TEMP= 0.000E+00   EPS  = -0.122E-06  0.329E-06 -0.574E-07
                            EPSP =  0.000E+00  0.000E+00  0.000E+00  0.000E+00  0.000E+00
                            SIGMA= -0.363E+04  0.358E+05  0.204E+04  0.330E+04 -0.873E+02

NCELL= 1  NSUB=5  (2,1,1)   JJ1= 1  X1= 0.234E-03
          TEMP= 0.000E+00   EPS  = -0.487E-07  0.176E-06 -0.574E-07
                            EPSP =  0.000E+00  0.000E+00  0.000E+00  0.000E+00  0.000E+00
                            SIGMA= -0.443E+04  0.674E+05 -0.720E+04  0.405E+03 -0.142E+03

NCELL= 1  NSUB=5  (2,1,1)   JJ1= 3  X1= 0.638E-03
          TEMP= 0.000E+00   EPS  = -0.491E-07  0.175E-06 -0.574E-07
                            EPSP =  0.000E+00  0.000E+00  0.000E+00  0.000E+00  0.000E+00
                            SIGMA= -0.475E+04  0.670E+05 -0.739E+04  0.405E+03 -0.142E+03

NCELL= 1  NSUB=5  (2,1,1)   JJ1= 5  X1= 0.104E-02
          TEMP= 0.000E+00   EPS  = -0.495E-07  0.174E-06 -0.574E-07
                            EPSP =  0.000E+00  0.000E+00  0.000E+00  0.000E+00  0.000E+00
                            SIGMA= -0.508E+04  0.665E+05 -0.758E+04  0.405E+03 -0.142E+03

.
.
.

NCELL= 5  NSUB=1  (1,1,1)   JJ1= 1  X1= 0.487E-02
          TEMP= 0.000E+00   EPS  = -0.884E-07  0.265E-06 -0.575E-07
                            EPSP =  0.000E+00  0.000E+00  0.000E+00  0.000E+00  0.000E+00
                            SIGMA= -0.208E+04  0.289E+05  0.622E+03 -0.301E+04 -0.821E+02

NCELL= 5  NSUB=1  (1,1,1)   JJ1= 3  X1= 0.498E-02
          TEMP= 0.000E+00   EPS  = -0.805E-07  0.265E-06 -0.575E-07
                            EPSP =  0.000E+00  0.000E+00  0.000E+00  0.000E+00  0.000E+00
                            SIGMA= -0.104E+04  0.292E+05  0.978E+03 -0.301E+04 -0.821E+02

NCELL= 5  NSUB=1  (1,1,1)   JJ1= 5  X1= 0.510E-02
```

```
          TEMP= 0.000E+00   EPS  = -0.727E-07  0.264E-06 -0.575E-07
                            EPSP =  0.000E+00  0.000E+00  0.000E+00  0.000E+00  0.000E+00
                            SIGMA=  0.163E+01  0.295E+05  0.134E+04 -0.301E+04 -0.821E+02

NCELL= 5  NSUB=5  (2,1,1)   JJ1= 1  X1= 0.510E-02
          TEMP= 0.000E+00   EPS  = -0.675E-07  0.260E-06 -0.574E-07
                            EPSP =  0.000E+00  0.000E+00  0.000E+00  0.000E+00  0.000E+00
                            SIGMA= -0.345E-01  0.105E+06  0.323E+04 -0.976E+04 -0.140E+03

NCELL= 5  NSUB=5  (2,1,1)   JJ1= 3  X1= 0.510E-02
          TEMP= 0.000E+00   EPS  = -0.675E-07  0.260E-06 -0.574E-07
                            EPSP =  0.000E+00  0.000E+00  0.000E+00  0.000E+00  0.000E+00
                            SIGMA= -0.173E-01  0.105E+06  0.323E+04 -0.976E+04 -0.140E+03

NCELL= 5  NSUB=5  (2,1,1)   JJ1= 5  X1= 0.510E-02
          TEMP= 0.000E+00   EPS  = -0.675E-07  0.260E-06 -0.574E-07
                            EPSP =  0.000E+00  0.000E+00  0.000E+00  0.000E+00  0.000E+00
                            SIGMA=  0.924E-10  0.105E+06  0.323E+04 -0.976E+04 -0.140E+03

AVERAGE TEMP. DEVIATION = DTEMPB=  0.000E+00
AVERAGE STRAIN=   -0.720E-07 -0.678E-21 -0.574E-07
AVERAGE STRESS=    0.748E+02  0.507E+05 -0.381E-09


             INCREMENT=  25

NCELL= 1  NSUB=1  (1,1,1)   JJ1= 1  X1= 0.000E+00
          TEMP= 0.000E+00   EPS  = -0.604E-04  0.208E-03 -0.359E-04
                            EPSP =  0.000E+00  0.000E+00  0.000E+00  0.000E+00  0.000E+00
                            SIGMA= -0.196E-01  0.235E+08  0.215E+07  0.207E+07 -0.546E+05

NCELL= 1  NSUB=1  (1,1,1)   JJ1= 3  X1= 0.117E-03
          TEMP= 0.000E+00   EPS  = -0.684E-04  0.207E-03 -0.359E-04
                            EPSP =  0.000E+00  0.000E+00  0.000E+00  0.000E+00  0.000E+00
                            SIGMA= -0.113E+07  0.229E+08  0.171E+07  0.207E+07 -0.546E+05

NCELL= 1  NSUB=1  (1,1,1)   JJ1= 5  X1= 0.234E-03
          TEMP= 0.000E+00   EPS  = -0.764E-04  0.205E-03 -0.359E-04
                            EPSP =  0.000E+00  0.000E+00  0.000E+00  0.000E+00  0.000E+00
                            SIGMA= -0.227E+07  0.224E+08  0.128E+07  0.207E+07 -0.546E+05

NCELL= 1  NSUB=5  (2,1,1)   JJ1= 1  X1= 0.234E-03
          TEMP= 0.000E+00   EPS  = -0.304E-04  0.110E-03 -0.359E-04
                            EPSP =  0.000E+00  0.000E+00  0.000E+00  0.000E+00  0.000E+00
                            SIGMA= -0.277E+07  0.421E+08 -0.450E+07  0.253E+06 -0.890E+05

NCELL= 1  NSUB=5  (2,1,1)   JJ1= 3  X1= 0.638E-03
          TEMP= 0.000E+00   EPS  = -0.307E-04  0.109E-03 -0.359E-04
                            EPSP =  0.000E+00  0.000E+00  0.000E+00  0.000E+00  0.000E+00
                            SIGMA= -0.297E+07  0.419E+08 -0.462E+07  0.253E+06 -0.890E+05

NCELL= 1  NSUB=5  (2,1,1)   JJ1= 5  X1= 0.104E-02
          TEMP= 0.000E+00   EPS  = -0.310E-04  0.109E-03 -0.359E-04
                            EPSP =  0.000E+00  0.000E+00  0.000E+00  0.000E+00  0.000E+00
                            SIGMA= -0.317E+07  0.416E+08 -0.474E+07  0.253E+06 -0.890E+05

.
.
.

NCELL= 5  NSUB=1  (1,1,1)   JJ1= 1  X1= 0.487E-02
          TEMP= 0.000E+00   EPS  = -0.552E-04  0.166E-03 -0.359E-04
                            EPSP =  0.000E+00  0.000E+00  0.000E+00  0.000E+00  0.000E+00
                            SIGMA= -0.130E+07  0.180E+08  0.389E+06 -0.188E+07 -0.513E+05

NCELL= 5  NSUB=1  (1,1,1)   JJ1= 3  X1= 0.498E-02
          TEMP= 0.000E+00   EPS  = -0.503E-04  0.165E-03 -0.359E-04
                            EPSP =  0.000E+00  0.000E+00  0.000E+00  0.000E+00  0.000E+00
                            SIGMA= -0.651E+06  0.182E+08  0.611E+06 -0.188E+07 -0.513E+05
```

```
NCELL= 5  NSUB=1  (1,1,1)   JJ1= 5  X1= 0.510E-02
          TEMP= 0.000E+00   EPS  = -0.454E-04  0.165E-03 -0.359E-04
                            EPSP =  0.000E+00  0.000E+00  0.000E+00  0.000E+00  0.000E+00
                            SIGMA=  0.102E+04  0.184E+08  0.835E+06 -0.188E+07 -0.513E+05

NCELL= 5  NSUB=5  (2,1,1)   JJ1= 1  X1= 0.510E-02
          TEMP= 0.000E+00   EPS  = -0.422E-04  0.162E-03 -0.359E-04
                            EPSP =  0.000E+00  0.000E+00  0.000E+00  0.000E+00  0.000E+00
                            SIGMA= -0.216E+02  0.655E+08  0.202E+07 -0.610E+07 -0.873E+05

NCELL= 5  NSUB=5  (2,1,1)   JJ1= 3  X1= 0.510E-02
          TEMP= 0.000E+00   EPS  = -0.422E-04  0.162E-03 -0.359E-04
                            EPSP =  0.000E+00  0.000E+00  0.000E+00  0.000E+00  0.000E+00
                            SIGMA= -0.108E+02  0.655E+08  0.202E+07 -0.610E+07 -0.873E+05

NCELL= 5  NSUB=5  (2,1,1)   JJ1= 5  X1= 0.510E-02
          TEMP= 0.000E+00   EPS  = -0.422E-04  0.162E-03 -0.359E-04
                            EPSP =  0.000E+00  0.000E+00  0.000E+00  0.000E+00  0.000E+00
                            SIGMA= -0.355E-06  0.655E+08  0.202E+07 -0.610E+07 -0.873E+05

AVERAGE TEMP. DEVIATION = DTEMPB=  0.000E+00
AVERAGE STRAIN=   -0.450E-04 -0.441E-17 -0.359E-04
AVERAGE STRESS=    0.467E+05  0.317E+08 -0.451E-06


              INCREMENT=  50

NCELL= 1  NSUB=1  (1,1,1)   JJ1= 1  X1= 0.000E+00
          TEMP= 0.000E+00   EPS  = -0.242E-03  0.831E-03 -0.143E-03
                            EPSP =  0.000E+00  0.000E+00  0.000E+00  0.000E+00  0.000E+00
                            SIGMA= -0.782E-01  0.939E+08  0.860E+07  0.826E+07 -0.218E+06

NCELL= 1  NSUB=1  (1,1,1)   JJ1= 3  X1= 0.117E-03
          TEMP= 0.000E+00   EPS  = -0.274E-03  0.826E-03 -0.143E-03
                            EPSP =  0.000E+00  0.000E+00  0.000E+00  0.000E+00  0.000E+00
                            SIGMA= -0.453E+07  0.918E+08  0.686E+07  0.826E+07 -0.218E+06

NCELL= 1  NSUB=1  (1,1,1)   JJ1= 5  X1= 0.234E-03
          TEMP= 0.000E+00   EPS  = -0.305E-03  0.821E-03 -0.143E-03
                            EPSP =  0.000E+00  0.000E+00  0.000E+00  0.000E+00  0.000E+00
                            SIGMA= -0.907E+07  0.896E+08  0.511E+07  0.826E+07 -0.218E+06

NCELL= 1  NSUB=5  (2,1,1)   JJ1= 1  X1= 0.234E-03
          TEMP= 0.000E+00   EPS  = -0.122E-03  0.440E-03 -0.143E-03
                            EPSP =  0.000E+00  0.000E+00  0.000E+00  0.000E+00  0.000E+00
                            SIGMA= -0.111E+08  0.168E+09 -0.180E+08  0.101E+07 -0.356E+06

NCELL= 1  NSUB=5  (2,1,1)   JJ1= 3  X1= 0.638E-03
          TEMP= 0.000E+00   EPS  = -0.123E-03  0.438E-03 -0.143E-03
                            EPSP =  0.000E+00  0.000E+00  0.000E+00  0.000E+00  0.000E+00
                            SIGMA= -0.119E+08  0.167E+09 -0.185E+08  0.101E+07 -0.356E+06

NCELL= 1  NSUB=5  (2,1,1)   JJ1= 5  X1= 0.104E-02
          TEMP= 0.000E+00   EPS  = -0.124E-03  0.436E-03 -0.143E-03
                            EPSP =  0.000E+00  0.000E+00  0.000E+00  0.000E+00  0.000E+00
                            SIGMA= -0.127E+08  0.166E+09 -0.190E+08  0.101E+07 -0.356E+06

.
.
.

NCELL= 5  NSUB=1  (1,1,1)   JJ1= 1  X1= 0.487E-02
          TEMP= 0.000E+00   EPS  = -0.221E-03  0.663E-03 -0.144E-03
                            EPSP =  0.000E+00  0.000E+00  0.000E+00  0.000E+00  0.000E+00
                            SIGMA= -0.521E+07  0.721E+08  0.155E+07 -0.753E+07 -0.205E+06

NCELL= 5  NSUB=1  (1,1,1)   JJ1= 3  X1= 0.498E-02
          TEMP= 0.000E+00   EPS  = -0.201E-03  0.662E-03 -0.144E-03
                            EPSP =  0.000E+00  0.000E+00  0.000E+00  0.000E+00  0.000E+00
                            SIGMA= -0.261E+07  0.729E+08  0.245E+07 -0.753E+07 -0.205E+06
```

```
NCELL= 5  NSUB=1  (1,1,1)   JJ1= 5  X1= 0.510E-02
          TEMP= 0.000E+00   EPS  = -0.182E-03  0.661E-03 -0.144E-03
                            EPSP =  0.000E+00  0.000E+00  0.000E+00  0.000E+00  0.000E+00
                            SIGMA=  0.408E+04  0.738E+08  0.334E+07 -0.753E+07 -0.205E+06

NCELL= 5  NSUB=5  (2,1,1)   JJ1= 1  X1= 0.510E-02
          TEMP= 0.000E+00   EPS  = -0.169E-03  0.650E-03 -0.144E-03
                            EPSP =  0.000E+00  0.000E+00  0.000E+00  0.000E+00  0.000E+00
                            SIGMA= -0.864E+02  0.262E+09  0.807E+07 -0.244E+08 -0.349E+06

NCELL= 5  NSUB=5  (2,1,1)   JJ1= 3  X1= 0.510E-02
          TEMP= 0.000E+00   EPS  = -0.169E-03  0.650E-03 -0.144E-03
                            EPSP =  0.000E+00  0.000E+00  0.000E+00  0.000E+00  0.000E+00
                            SIGMA= -0.432E+02  0.262E+09  0.807E+07 -0.244E+08 -0.349E+06

NCELL= 5  NSUB=5  (2,1,1)   JJ1= 5  X1= 0.510E-02
          TEMP= 0.000E+00   EPS  = -0.169E-03  0.650E-03 -0.144E-03
                            EPSP =  0.000E+00  0.000E+00  0.000E+00  0.000E+00  0.000E+00
                            SIGMA= -0.142E-05  0.262E+09  0.807E+07 -0.244E+08 -0.349E+06

AVERAGE TEMP. DEVIATION = DTEMPB=  0.000E+00
AVERAGE STRAIN=    -0.180E-03 -0.176E-16 -0.144E-03
AVERAGE STRESS=     0.187E+06  0.127E+09 -0.180E-05


             INCREMENT=  75

NCELL= 1  NSUB=1  (1,1,1)   JJ1= 1  X1= 0.000E+00
          TEMP= 0.000E+00   EPS  = -0.544E-03  0.187E-02 -0.323E-03
                            EPSP =  0.000E+00  0.000E+00  0.000E+00  0.000E+00  0.000E+00
                            SIGMA= -0.176E+00  0.211E+09  0.194E+08  0.186E+08 -0.491E+06

NCELL= 1  NSUB=1  (1,1,1)   JJ1= 3  X1= 0.117E-03
          TEMP= 0.000E+00   EPS  = -0.615E-03  0.186E-02 -0.323E-03
                            EPSP =  0.000E+00  0.000E+00  0.000E+00  0.000E+00  0.000E+00
                            SIGMA= -0.102E+08  0.206E+09  0.154E+08  0.186E+08 -0.491E+06

NCELL= 1  NSUB=1  (1,1,1)   JJ1= 5  X1= 0.234E-03
          TEMP= 0.000E+00   EPS  = -0.687E-03  0.185E-02 -0.323E-03
                            EPSP =  0.000E+00  0.000E+00  0.000E+00  0.000E+00  0.000E+00
                            SIGMA= -0.204E+08  0.202E+09  0.115E+08  0.186E+08 -0.491E+06

NCELL= 1  NSUB=5  (2,1,1)   JJ1= 1  X1= 0.234E-03
          TEMP= 0.000E+00   EPS  = -0.274E-03  0.989E-03 -0.323E-03
                            EPSP =  0.000E+00  0.000E+00  0.000E+00  0.000E+00  0.000E+00
                            SIGMA= -0.249E+08  0.379E+09 -0.405E+08  0.228E+07 -0.801E+06

NCELL= 1  NSUB=5  (2,1,1)   JJ1= 3  X1= 0.638E-03
          TEMP= 0.000E+00   EPS  = -0.276E-03  0.985E-03 -0.323E-03
                            EPSP =  0.000E+00  0.000E+00  0.000E+00  0.000E+00  0.000E+00
                            SIGMA= -0.267E+08  0.377E+09 -0.416E+08  0.228E+07 -0.801E+06

NCELL= 1  NSUB=5  (2,1,1)   JJ1= 5  X1= 0.104E-02
          TEMP= 0.000E+00   EPS  = -0.279E-03  0.980E-03 -0.323E-03
                            EPSP =  0.000E+00  0.000E+00  0.000E+00  0.000E+00  0.000E+00
                            SIGMA= -0.286E+08  0.374E+09 -0.426E+08  0.228E+07 -0.801E+06

.
.
.

NCELL= 5  NSUB=1  (1,1,1)   JJ1= 1  X1= 0.487E-02
          TEMP= 0.000E+00   EPS  = -0.497E-03  0.149E-02 -0.323E-03
                            EPSP =  0.000E+00  0.000E+00  0.000E+00  0.000E+00  0.000E+00
                            SIGMA= -0.117E+08  0.162E+09  0.350E+07 -0.169E+08 -0.462E+06

NCELL= 5  NSUB=1  (1,1,1)   JJ1= 3  X1= 0.498E-02
          TEMP= 0.000E+00   EPS  = -0.453E-03  0.149E-02 -0.323E-03
                            EPSP =  0.000E+00  0.000E+00  0.000E+00  0.000E+00  0.000E+00
                            SIGMA= -0.586E+07  0.164E+09  0.550E+07 -0.169E+08 -0.462E+06
```

```
NCELL= 5  NSUB=1  (1,1,1)   JJ1= 5  X1= 0.510E-02
          TEMP= 0.000E+00   EPS  = -0.409E-03  0.149E-02 -0.323E-03
                            EPSP =  0.000E+00  0.000E+00  0.000E+00  0.000E+00  0.000E+00
                            SIGMA=  0.917E+04  0.166E+09  0.751E+07 -0.169E+08 -0.462E+06

NCELL= 5  NSUB=5  (2,1,1)   JJ1= 1  X1= 0.510E-02
          TEMP= 0.000E+00   EPS  = -0.380E-03  0.146E-02 -0.323E-03
                            EPSP =  0.000E+00  0.000E+00  0.000E+00  0.000E+00  0.000E+00
                            SIGMA= -0.194E+03  0.589E+09  0.182E+08 -0.549E+08 -0.785E+06

NCELL= 5  NSUB=5  (2,1,1)   JJ1= 3  X1= 0.510E-02
          TEMP= 0.000E+00   EPS  = -0.380E-03  0.146E-02 -0.323E-03
                            EPSP =  0.000E+00  0.000E+00  0.000E+00  0.000E+00  0.000E+00
                            SIGMA= -0.972E+02  0.589E+09  0.182E+08 -0.549E+08 -0.785E+06

NCELL= 5  NSUB=5  (2,1,1)   JJ1= 5  X1= 0.510E-02
          TEMP= 0.000E+00   EPS  = -0.380E-03  0.146E-02 -0.323E-03
                            EPSP =  0.000E+00  0.000E+00  0.000E+00  0.000E+00  0.000E+00
                            SIGMA=  0.321E-05  0.589E+09  0.182E+08 -0.549E+08 -0.785E+06

AVERAGE TEMP. DEVIATION = DTEMPB=  0.000E+00
AVERAGE STRAIN=   -0.405E-03  0.927E-17 -0.323E-03
AVERAGE STRESS=    0.420E+06  0.285E+09  0.336E-05


              INCREMENT= 100

NCELL= 1  NSUB=1  (1,1,1)   JJ1= 1  X1= 0.000E+00
          TEMP= 0.000E+00   EPS  = -0.194E-02  0.483E-02 -0.737E-03
                            EPSP = -0.709E-03  0.113E-02 -0.423E-03 -0.875E-20 -0.119E-22
                            SIGMA=  0.314E+06  0.416E+09  0.786E+08  0.725E+08 -0.816E+06
                            EFF. STRESSES=  0.398E+09  0.403E+09

NCELL= 1  NSUB=1  (1,1,1)   JJ1= 3  X1= 0.117E-03
          TEMP= 0.000E+00   EPS  = -0.229E-02  0.480E-02 -0.737E-03
                            EPSP = -0.825E-03  0.125E-02 -0.420E-03 -0.193E-19  0.485E-23
                            SIGMA= -0.380E+08  0.386E+09  0.598E+08  0.725E+08 -0.816E+06
                            EFF. STRESSES=  0.401E+09  0.404E+09

NCELL= 1  NSUB=1  (1,1,1)   JJ1= 5  X1= 0.234E-03
          TEMP= 0.000E+00   EPS  = -0.264E-02  0.477E-02 -0.737E-03
                            EPSP = -0.949E-03  0.136E-02 -0.411E-03 -0.143E-19 -0.300E-22
                            SIGMA= -0.757E+08  0.356E+09  0.406E+08  0.725E+08 -0.816E+06
                            EFF. STRESSES=  0.404E+09  0.407E+09

NCELL= 1  NSUB=5  (2,1,1)   JJ1= 1  X1= 0.234E-03
          TEMP= 0.000E+00   EPS  = -0.526E-03  0.177E-02 -0.736E-03
                            EPSP =  0.000E+00  0.000E+00  0.000E+00  0.000E+00  0.000E+00
                            SIGMA= -0.865E+08  0.649E+09 -0.154E+09  0.891E+07 -0.151E+07

NCELL= 1  NSUB=5  (2,1,1)   JJ1= 3  X1= 0.638E-03
          TEMP= 0.000E+00   EPS  = -0.546E-03  0.176E-02 -0.736E-03
                            EPSP =  0.000E+00  0.000E+00  0.000E+00  0.000E+00  0.000E+00
                            SIGMA= -0.973E+08  0.642E+09 -0.158E+09  0.891E+07 -0.151E+07

NCELL= 1  NSUB=5  (2,1,1)   JJ1= 5  X1= 0.104E-02
          TEMP= 0.000E+00   EPS  = -0.565E-03  0.176E-02 -0.736E-03
                            EPSP =  0.000E+00  0.000E+00  0.000E+00  0.000E+00  0.000E+00
                            SIGMA= -0.108E+09  0.635E+09 -0.163E+09  0.891E+07 -0.151E+07

.
.
.

NCELL= 5  NSUB=1  (1,1,1)   JJ1= 1  X1= 0.487E-02
          TEMP= 0.000E+00   EPS  = -0.149E-02  0.354E-02 -0.738E-03
                            EPSP = -0.167E-03  0.271E-03 -0.104E-03 -0.440E-21  0.636E-24
                            SIGMA= -0.491E+08  0.341E+09  0.947E+07 -0.634E+08 -0.807E+06
                            EFF. STRESSES=  0.378E+09  0.381E+09
```

```
NCELL= 5  NSUB=1  (1,1,1)   JJ1= 3  X1= 0.498E-02
          TEMP= 0.000E+00   EPS  = -0.127E-02  0.353E-02 -0.738E-03
                            EPSP = -0.117E-03  0.199E-03 -0.824E-04 -0.137E-21 -0.108E-23
                            SIGMA= -0.247E+08  0.357E+09  0.179E+08 -0.634E+08 -0.807E+06
                            EFF. STRESSES=  0.376E+09  0.378E+09

NCELL= 5  NSUB=1  (1,1,1)   JJ1= 5  X1= 0.510E-02
          TEMP= 0.000E+00   EPS  = -0.105E-02  0.353E-02 -0.738E-03
                            EPSP = -0.734E-04  0.133E-03 -0.593E-04 -0.315E-21  0.164E-23
                            SIGMA=  0.392E+06  0.372E+09  0.262E+08 -0.634E+08 -0.807E+06
                            EFF. STRESSES=  0.375E+09  0.376E+09

NCELL= 5  NSUB=5  (2,1,1)   JJ1= 1  X1= 0.510E-02
          TEMP= 0.000E+00   EPS  = -0.870E-03  0.335E-02 -0.737E-03
                            EPSP =  0.000E+00  0.000E+00  0.000E+00  0.000E+00  0.000E+00
                            SIGMA= -0.794E+03  0.135E+10  0.427E+08 -0.222E+09 -0.137E+07

NCELL= 5  NSUB=5  (2,1,1)   JJ1= 3  X1= 0.510E-02
          TEMP= 0.000E+00   EPS  = -0.870E-03  0.335E-02 -0.737E-03
                            EPSP =  0.000E+00  0.000E+00  0.000E+00  0.000E+00  0.000E+00
                            SIGMA= -0.397E+03  0.135E+10  0.427E+08 -0.222E+09 -0.137E+07

NCELL= 5  NSUB=5  (2,1,1)   JJ1= 5  X1= 0.510E-02
          TEMP= 0.000E+00   EPS  = -0.870E-03  0.335E-02 -0.737E-03
                            EPSP =  0.000E+00  0.000E+00  0.000E+00  0.000E+00  0.000E+00
                            SIGMA=  0.545E-05  0.135E+10  0.427E+08 -0.222E+09 -0.137E+07

AVERAGE TEMP. DEVIATION = DTEMPB=  0.000E+00
AVERAGE STRAIN=   -0.123E-02 -0.226E-16 -0.737E-03
AVERAGE STRESS=   -0.854E+06  0.518E+09  0.651E+05

           END OF JOB
```

7.4 Appendix 4

The input data file *fgmp.tube.opt.data.initial* defines the optimization problem and contains information on the initial values of the design variables as describes in section 3.2. Its structure, the variable names and their description read by the program are given below.

ICASE	axial constraint indicator: 1 -> plane strain constraint; 2 -> generalized plane strain constraint
METHODM	method of optimization used within *DOT*: 1 -> method of feasible directions
MINMAX	indicates whether the user-defined objective function is to be minimized or maximized: -1 -> minimized; 1 -> maximized
HH	total cylinder thickness
DF	radial fiber dimension
	begin specification of initial reinforcement spacing --> repeat NDV (number of design variables) times
I,X	design variable number, initial spacing between reinforcement
	end of initial reinforcement spacing specifications

The inut file *fgmp.tube.opt.data* is organized into four distinct blocks, as explained in section 3.2, along the same lines as those for *fgmp.tube.data*. The structure of these input data files, the variable names and their description read by the program are given below.

Block 1: Material properties for NMT materials at NTEMP identical temperatures

The names and sequence of the variables employed in this block are identical to those in the corresponding block of the file *fgmp.tube.data* given in Appendix 1.

Block 2: Loading specification and write options

TREF	reference temperature
AMPTOPT,AMPBOTT	maximum temperatures applied at the top and bottom surfaces
LOADTOPM,LOADBOTM	mechanical loading type indicators for top and bottom surfaces: 1 -> radial traction; 2 -> radial displacement

AMPTOPM,AMPBOTM	maximum values of mechanical loading (radial traction/displacement)
ISW,FLOAD	axial constraint indicator, magnitude of axial load: ISW=1 -> average axial strain imposed; ISW=2 -> average axial stress imposed
OMEGAF	magnitude of steady-state angular velocity
NINT,NINA	total number of load increments used in the solution of equations (4) and (13) -> defines load increment size; actual number of load increments
MAXITERATION	number of iterations used in the solution of equation (13) at each load increment
JPLOT,KPLOT	specification of the subcells β, γ through which output results are written to the *fgmp.tube.plot* file

Block 3: Specification of the cylinder architecture and geometry

M	number of cells in the radial direction
DF,HH	radial fiber dimension, total cylinder thickness
NTHETA,H1H2,R0	number of cells along the θ-direction, ratio of the subcell dimensions h_1/h_2, inner radius of the cylinder
L1,L2	subcell dimensions l_1 and l_2
	begin subcell material assignment --> repeat M times
NCELL1,MATNUM	cell number, material assignment in the eight subcells (1 1 1) --> (2 2 2) of each cell
	end of subcell material assignment for M cells

Block 4: Specification of the approximation of integration of the plastic strain field in the individual subcells in equation (13)

The names and sequence of the variables employed in this block are identical to those in the corresponding block of the file *fgmp.tube.data* given in Appendix 1.

7.5 Appendix 5

The input file *fgmp.tube.data.initial* for the case described in section 4.3.2 is given below, with the actual variable names (not to be included in the input deck) given on the right in block letters.

```
 2                                                    ICASE
 1                                                    METHODM
-1                                                    MINMAX
 5.1E-3                                               HH
 0.8062E-3                                            DF
 1    0.2344E-3                                       I,X
 2    0.4688E-3                                       .
 3    0.4688E-3                                       .
 4    0.4688E-3                                       .
 5    0.2344E-3                                       .
```

The input file *fgmp.tube.data* for the case described in section 4.3.2 is given below, with the highlighted text identifying the four blocks of the input data and the actual variable names (not to be included in the input deck) given on the right in block letters.

Block 1

```
 2                                                    NMAT
 SiC                                                  MNAME
 1                                                    ID
 1                                                    NTEMP
 1     0.0E+00                                        IT1,TEMP
 8.0   8.0                                            CONDATEMP,CONDTTEMP
 399.90E+09    399.90E+09   159.96E+09                EATEMP,ETTEMP,GATEMP
   0.25E+00      0.25E+00                            FNATEMP,FNTTEMP
   1.00E-06      1.00E-06                            ALPATEMP,ALPTTEMP
   0.00E+06     23.00E+09                            YIELDTEMP,HARDTEMP

 Ti
 1
 1
 1     0.0E+00
 8.0           8.0
 110.30E+09    110.30E+09     43.77E+09
 0.26E+00      0.26E+00
 1.00E-06      1.00E-06
 71.60E+06     23.00E+09
```

Block 2

```
  0                                                  TREF
  0        0                                         AMPTOPT,AMPBOTT
  1        1                                         LOADTOPM,LOADBOTM
  0        0.                                        AMPTOPM,AMPBOTM
  2        0.                                        ISW,FLOAD
  7700E2                                             OMEGAF
  100      100                                       NINT,NINA
  10                                                 MAXITERATION
  1    1                                             JPLOT,KPLOT
```

Block 3

```
5                                                    M
0.8062E-3       5.1E-3                               DF,HH
125       1.72              25.4E-3                  NTHETA,H1H2,R0
0.8062E-3     0.4688E-3                              L1,L2
1      2 2 2 2 1 1 2 2                               NCELL1,MATNUM(1,1,1)...MATNUM(2,2,2)
2      2 2 2 2 1 1 2 2                               .
3      2 2 2 2 1 1 2 2                               .
4      2 2 2 2 1 1 2 2                               .
5      2 2 2 2 1 1 1 1                               .
```

Block 4

```
2  2  2                                              NLEG1,NLEG2,NLEG3
5  5  5                                              J1,J2,J3
```

REPORT DOCUMENTATION PAGE

Form Approved
OMB No. 0704-0188

1. AGENCY USE ONLY (*Leave blank*)	2. REPORT DATE	3. REPORT TYPE AND DATES COVERED
	June 1998	Final Contractor Report

4. TITLE AND SUBTITLE

HOTCFGM-1D: A Coupled Higher-Order Theory for Cylindrical Structural Components With Through-Thickness Functionally Graded Microstructures

5. FUNDING NUMBERS

WU-523-90-13-00
NAS3-96052

6. AUTHOR(S)

Marek-Jerzy Pindera and Jacob Aboudi

7. PERFORMING ORGANIZATION NAME(S) AND ADDRESS(ES)

University of Virginia
Civil Engineering and Applied Mechanics Department
Charlottesville, Virginia 22903

8. PERFORMING ORGANIZATION REPORT NUMBER

E-11187

9. SPONSORING/MONITORING AGENCY NAME(S) AND ADDRESS(ES)

National Aeronautics and Space Administration
Lewis Research Center
Cleveland, Ohio 44135-3191

10. SPONSORING/MONITORING AGENCY REPORT NUMBER

NASA CR—1998-207927

11. SUPPLEMENTARY NOTES

Marek-Jerzy Pindera, University of Virginia, Civil Engineering and Applied Mechanics Department, Charlottesville, Virginia 22903, and Jacob Aboudi, Visiting Professor, Faculty of Engineering, Tel-Aviv University, Ramat-Aviv, Tel-Aviv 69978, Israel. Project Manager, Steven M. Arnold, Structures and Acoustics Division, NASA Lewis Research Center, organization code 5920, (216) 433-3334.

12a. DISTRIBUTION/AVAILABILITY STATEMENT

Unclassified - Unlimited
Subject Categories: 24 and 39 Distribution: Nonstandard

This publication is available from the NASA Center for AeroSpace Information, (301) 621-0390.

12b. DISTRIBUTION CODE

13. ABSTRACT ***(Maximum 200 words)***

This report summarizes the work performed under the contract NAS3-96052 during the FY97 funding period. The objective of this three-year project was to develop and deliver to NASA Lewis one-dimensional and two-dimensional higher-order theories, and related computer codes, for the analysis, optimization and design of cylindrical functionally graded materials/structural components for use in advanced aircraft engines (e.g., combustor linings, rotor disks, heat shields, blisk blades). To satisfy this objective, a quasi one-dimensional version of the higher-order theory, HOTCFGM-1D, and four computer codes based on this theory, for the analysis, design and optimization of cylindrical structural components functionally graded in the radial direction were developed. The theory is applicable to thin multi-phased composite shells/cylinders subjected to macroscopically axisymmetric thermomechanical and inertial loading applied uniformly along the axial direction such that the overall deformation is characterized by a constant average axial strain. The reinforcement phases are uniformly distributed in the axial and circumferential directions, and arbitrarily distributed in the radial direction, thereby allowing functional grading of the internal reinforcement in this direction.

14. SUBJECT TERMS

Composites; Cylindrical; Functionally graded materials; Optimization; Inelasticity

15. NUMBER OF PAGES

58

16. PRICE CODE

A04

17. SECURITY CLASSIFICATION OF REPORT	18. SECURITY CLASSIFICATION OF THIS PAGE	19. SECURITY CLASSIFICATION OF ABSTRACT	20. LIMITATION OF ABSTRACT
Unclassified	Unclassified	Unclassified	